International Journal of Hydrogen Energy 194 (2025) 152508

Contents lists available at ScienceDirect

International Journal of Hydrogen Energy

journal homepage: www.elsevier.com/locate/he

A pathway to decarbonizing cement manufacturing via solar-driven green hydrogen systems

Sobit Sapkota [a], Anup Paudel [a], Wonjae Choi [b], Inyoung Ko [b], Jun-Ki Choi [a,c,*]

[a] Department of Mechanical Engineering, University of Dayton, OH, 45409, United States
[b] Mechanical and Biomedical Engineering, Ewha Womans University, Seoul, 03760, South Korea
[c] Renewable and Clean Energy Program, University of Dayton, OH, 45409, United States

ARTICLE INFO

Keywords:
Green hydrogen
cement industry
Solar energy integration
Techno-economic optimization
Industrial decarbonization

ABSTRACT

The cement industry, a foundation of infrastructure development, is responsible for nearly 7 % of global CO_2 emissions, highlighting an urgent need for scalable decarbonization strategies. This study investigates the techno-economic feasibility of integrating on-site solar-powered green hydrogen production into cement manufacturing processes. A mixed-integer linear programming (MILP) model optimizes the design and operation of solar photovoltaics (PV), proton exchange membrane (PEM) electrolyzer, and hydrogen storage for a representative cement plant in Texas. Five hydrogen substitution scenarios (10–30 % of thermal demand) were evaluated based on net present cost (NPC), levelized cost of hydrogen (LCOH), cost of CO_2 avoided and greenhouse gas (GHG) emissions reduction. Hydrogen integration up to 30 % is technically viable but economically constrained, with LCOH rising non-linearly from $58.7 to $95.3 GJ^{-1} due to escalating component costs. Environmentally, a 30 % hydrogen share could reduce total U.S. cement sector emissions by 22 %. While significant, this confirms at present, the solar-driven hydrogen serves as a partial solution rather than a standalone pathway to deep decarbonization, suggesting it must complement other strategies like carbon capture, electrification and other complementary technologies. The economic viability of this approach is entirely contingent on financial incentives as the investment tax credits of 80 % or higher are essential to enable cost parity with fossil fuels. This work provides a comprehensive techno-economic and environmental framework concluding immense economic barriers and that aggressive policy support is indispensable for enabling the transition to low-carbon cement manufacturing.

1. Introduction

The cement industry is a cornerstone of global infrastructure development and economic growth. As economies expand, cement production serves as a key indicator of rising infrastructure needs, forming the backbone of modern construction, enabling the creation of buildings, roads, bridges, and other vital structures [1]. With global cement production reaching 4.1 billion metric tons annually and expected to increase tenfold by 2050 [2], alongside U.S. production of around 90 million metric tons per year [3], demand continues to rise. Cement manufacturing is one of the most energy-intensive and high-emission industrial processes [4]. It is the third-largest industrial energy consumer [5], accounting for 10.7 EJ which equals to 7 % of the world's industrial energy consumption and contributing 2.2 Gt CO_2/year equaling 6–7 % of global anthropogenic CO_2 emissions [6,7]. Within the U.S. industrial sector, the cement industry alone produces 65.6 million metric tons of carbon dioxide equivalent annually accounting for nearly 4 % of U.S. industrial GHG emissions in 2023 with process emission of 39.7 million metric tons and fuel based emission of 25.9 million metric tons [8,9]. This significant carbon footprint, coupled with projected growth in cement demand, necessitates immediate and scalable decarbonization strategies to achieve net-zero emissions by 2050.

Cement manufacturing occurs in multiple stages, from raw material extraction and clinker formation to final cement production [10]. The primary component of cement, clinker [11], is produced through an energy-intensive process, with the kiln, preheater and calciner stages accounting around 90 % of energy consumption [12]. These same stages are responsible for the majority of CO_2 emissions as well. Clinker formation requires extreme temperatures of approximately 1450 °C [13], which are primarily generated by fossil fuel combustion, mainly coal

* Corresponding author. Department of Mechanical Engineering, University of Dayton, OH, 45409, United States.
E-mail address: jchoi1@udayton.edu (J.-K. Choi).

https://doi.org/10.1016/j.ijhydene.2025.152508
Received 28 April 2025; Received in revised form 3 November 2025; Accepted 8 November 2025
Available online 11 November 2025
0360-3199/© 2025 The Authors. Published by Elsevier Ltd on behalf of Hydrogen Energy Publications LLC. This is an open access article under the CC BY license (http://creativecommons.org/licenses/by/4.0/).

[14]. The process involves two key reactions: calcination, where limestone decomposes into CaO and CO_2 at 900 °C, and sintering, where CaO reacts with silica, alumina, and ferrous oxide at 1450 °C [15]. Fossil fuel combustion accounts for 40–45 % of the cement industry's total emissions, while calcination contributes 50–55 % of direct CO_2 emissions [16].

Decarbonizing the cement industry remains a significant challenge due to major emissions coming from widely available raw materials like limestone and crushed rock, along with long-established manufacturing technologies [17]. To address this issue, various carbon capture utilization and storage (CCUS) technologies are being explored, including post-combustion capture, oxy-combustion, and direct separation [18]. While effective, CCUS alone cannot fully mitigate emissions. The GCCA Net-Zero Roadmap estimates that CCUS could deliver about 36 % of total cumulative emission reductions required across the cement and concrete sector, corresponding to 3.8 Giga tons CO_2 by 2050 [19]. In practice, the capture rates of emissions are typically 85–90 % [20] but retrofitting all the cement industries are not physically and economically feasible, many sites lack access to suitable geological storage, and the energy and cost penalties limit universal deployment. CCUS is expected to play a major role but must be complemented by clinker substitution, fuel switching and low-carbon binders for deep decarbonization [21].

Fuel switching has long been practiced as a complementary decarbonization strategy, primarily to reduce reliance on coal and petroleum coke [22,23]. Several alternative fuels, such as waste oils, plastics, shredded residues, and waste tires, have been proposed and are primarily used as solid, liquid, and gas-based waste fuels [24]. These strategies have been motivated largely by cost savings and waste management benefits but continue to release CO_2 upon combustion. In the US cement industry, the current fuel mix is predominantly fossil fuels (coal 41 %, petroleum coke 24 %, natural gas 23 %, waste oils/tars 3 %, coke and breeze 1 %, distillate and residual fuels 1 %, and others 8 % [25]). To achieve deep decarbonization, a carbon-free alternative is therefore needed [26,27].

Hydrogen, with its potential for carbon-free emissions when produced renewably, is emerging as a promising alternative fuel [21]. As the cement industry seeks pathways to achieve net-zero emissions, green hydrogen presents a compelling solution, aligning with more aggressive sustainability strategies needed to decarbonize high-temperature industrial processes [28]. Produced via electrolysis powered by renewable energy [29,30], green hydrogen has an maximum emissions limit of just 36.4 g CO_2-eq/MJ [31]. Its integration into cement kilns could potentially reduce sectoral emissions by 34–40 % [32]. With a high calorific value (141.8 MJ/kg), approximately 6–7 times that of coal [33,34], hydrogen offers high combustion efficiency and potentially seamless integration into existing heat systems [35,36].

Transitioning to a low-carbon cement industry requires fuel switching with renewable energy integration alongside carbon capture technologies. This study investigates the techno-economic feasibility of green hydrogen by optimizing solar-powered production, storage, and utilization in clinker kiln-calciner system to minimize costs using a Mixed-Integer Linear Programming (MILP) model. The analysis optimizes the design and operation of a PV-electrolyzer-hydrogen storage system for a representative U.S. cement plant, evaluating system performance and costs across different hydrogen substitution levels. Environmental impacts are assessed through direct and indirect CO_2 reductions and the cost of CO_2 avoided. We also evaluate the role of policy incentives in improving financial competitiveness and scalability. By addressing these factors, this research provides data-driven insights to guide industry and policy decisions, accelerating decarbonization and supporting the cement sector's path to net-zero emissions by 2050.

2. Literature review

The cement industry's shift toward low-carbon alternatives has driven extensive research into hydrogen as a viable fuel replacement for high-temperature processes. Kilns and preheaters, responsible major energy consumption in industry [37], present a key opportunity for hydrogen integration. Studies demonstrate that hydrogen can be introduced into existing heat systems with minor modifications [38], allowing for progressive fuel substitution without major infrastructure overhauls.

Research has explored various approaches, including blending hydrogen with conventional fuels, co-firing with alternative fuels like refuse-derived fuel (RDF) and biomass [39], and using hydrogen-biofuel blends [40]. Blending hydrogen at levels of 5–20 % has demonstrated CO_2 emission reductions of up to 6 % equaling 22 Mt, often with minimal equipment changes. More substantial emission reductions, up to 21 % (about 70 Mt cumulative CO_2 savings), have been projected for biomass-hythane blends in the Canadian cement industry [41]. Industrial trials reinforce these findings. For instance, CEMEX has utilized hydrogen injection as a catalyst to optimize combustion and increase alternative fuel use, achieving a 34 % substitution rate [42]. HeidelbergCement's Ribblesdale plant achieved net-zero operation with a fuel mix containing 39 % hydrogen, biomass, and glycerine, confirming the feasibility of retrofitting burners for up to 40 % hydrogen blends [43]. These trials also showed that cement produced with hydrogen-biofuel blends exhibits comparable performance to that produced with traditional fossil fuels, despite some minor differences in clinker mineralogy and hydration [44].

Retrofitting burners for hydrogen combustion remains a key challenge due to hydrogen's distinct combustion characteristics, including higher flame speed, lower ignition energy, and unique temperature profiles [45]. To address these concerns, advanced burner technologies have been explored, such as pre-mixed flames, staged combustion, and porous media burners, which enhance stability and minimize flashback risks [46,47]. Programs like Hy4Heat emphasize material durability for high-temperature hydrogen use and highlight the need for rigorous safety protocols to mitigate unintended ignition risks [48].

Beyond combustion, research is also exploring various hydrogen production methods suitable for the cement industry. On-site ammonia cracking [49] and oxycombustion [50] offer practical solutions, simplifying storage and transport while potentially reducing CO_2 emissions by up to 44 %. Integrating hydrogen production with Power-to-Gas systems and CO_2 capture technologies has also been identified as a promising decarbonization pathway [51], although economic and technological hurdles remain.

Economic feasibility remains a key barrier to hydrogen adoption. To assess the trade-offs and viability of emerging technologies, many studies have employed techno-economic-environmental analyses [52]. While blending reduces emissions, it can increase production costs by 0.6 %–16 %, depending on the substitution rate [53]. Research into wind-alkaline electrolysis suggests hydrogen costs of $2.12–$2.26 per kg at $63 per MWh electricity [54], with projected reductions of 35 % by 2030 [55]. Studies on solar-electrolyzer integration further indicate potential cost reductions in levelized cost of hydrogen (LCOH) [56]. Despite technological advancements, hydrogen remains economically uncompetitive with fossil fuels without financial support.

The U.S. National Clean Hydrogen Strategy and Roadmap aims to bridge this cost gap through initiatives such as the Hydrogen Shot program, targeting $1 per kg hydrogen production by 2031 [57]. Policy incentives, including clean hydrogen production tax credits (45V, named after Section 45V of the U.S. Inflation Reduction Act of 2022) [58] and regional hydrogen hubs, play a crucial role in accelerating industry adoption. However, few studies directly analyze the impact of such incentives on cement production costs and higher hydrogen substitution rates.

To optimize the design and operation of these complex integrated systems, researchers have employed various modeling techniques. Studies have utilized models like linear optimization [59] and mixed-integer linear programming (MILP) to optimize hybrid renewable systems, including configurations with solar thermal [60,61],

photovoltaics [62], wind [63], desalination [64], water treatment [65,66], industrial energy [67,68] and hydrogen fuel cells [69,70]. These models focus on minimizing lifecycle costs while ensuring a reliable power supply to meet fluctuating demands.

While hydrogen has been considered as a potential fuel for various industries, no existing research has specifically addressed the integration of green hydrogen, produced from renewable energy sources, into the cement manufacturing process. Although several studies have investigated hydrogen use in cement production, many have focused on low substitution rates, the hydrogen used are not green with mainly derived from steam reforming or from gasification and also lack comprehensive techno-economic analyses. Much of the existing research does not explicitly address the challenges or system-level implications of using hydrogen derived from renewable sources. This study makes a novel contribution by addressing the unique technical and economic challenges of coupling solar-powered electrolysis with the continuous, high-temperature energy demands of cement production. This integration is particularly relevant for solar-rich, cement-intensive regions like Texas. The role of policy incentives in enhancing economic feasibility, such as investment tax credits, has also not been systematically evaluated in this context. To address these gaps, we develop a comprehensive techno-economic model using MILP to optimize a solar PV-powered hydrogen system integrated with weather data of representative climate zones. Through a techno-economic and environmental evaluation of multiple hydrogen substitution scenarios, this research offers one of the first in-depth assessments of green hydrogen's potential to decarbonize cement manufacturing.

3. Methodology

Fig. 1 outlines the step-by-step process used to design and optimize a renewable hydrogen production system for cement manufacturing. The study starts with data collection, where we gather information on industrial energy demands, solar availability, and economic factors to shape the system design. In system modeling, we develop mathematical representations of how solar PV generates power, how the electrolyzer produces hydrogen and how it is stored. The optimization phase forms the core of the study where a Mixed Integer Linear Programming (MILP) model is employed. MILP is a mathematical technique that simultaneously optimizes continuous variables (such as energy flows and production rates) and discrete decisions (like equipment sizing and on/off status) to determine the most cost-effective system configuration. It does this while considering key system constraints, such as solar resource availability, storage capacity, and plant operation needs, to ensure enough hydrogen is produced to replace coal under different scenarios. Finally, in post-analysis, we assess the economic feasibility, calculate GHG reductions for a typical cement plant, see the impact of policy in making the system economically viable, and also scale up the results to estimate the potential impact across the entire U.S. cement industry. This study evaluates five scenarios with annual hydrogen shares of 10 %, 15 %, 20 %, 25 %, and 30 % in the combined clinker kiln and calciner system.

Based on reported operating conditions of 900 °C in the calciner and 1450 °C in the rotary kiln [13], hydrogen blending ratios were capped at 45 % for the calciner and 25 % for the kiln. These values reflect findings

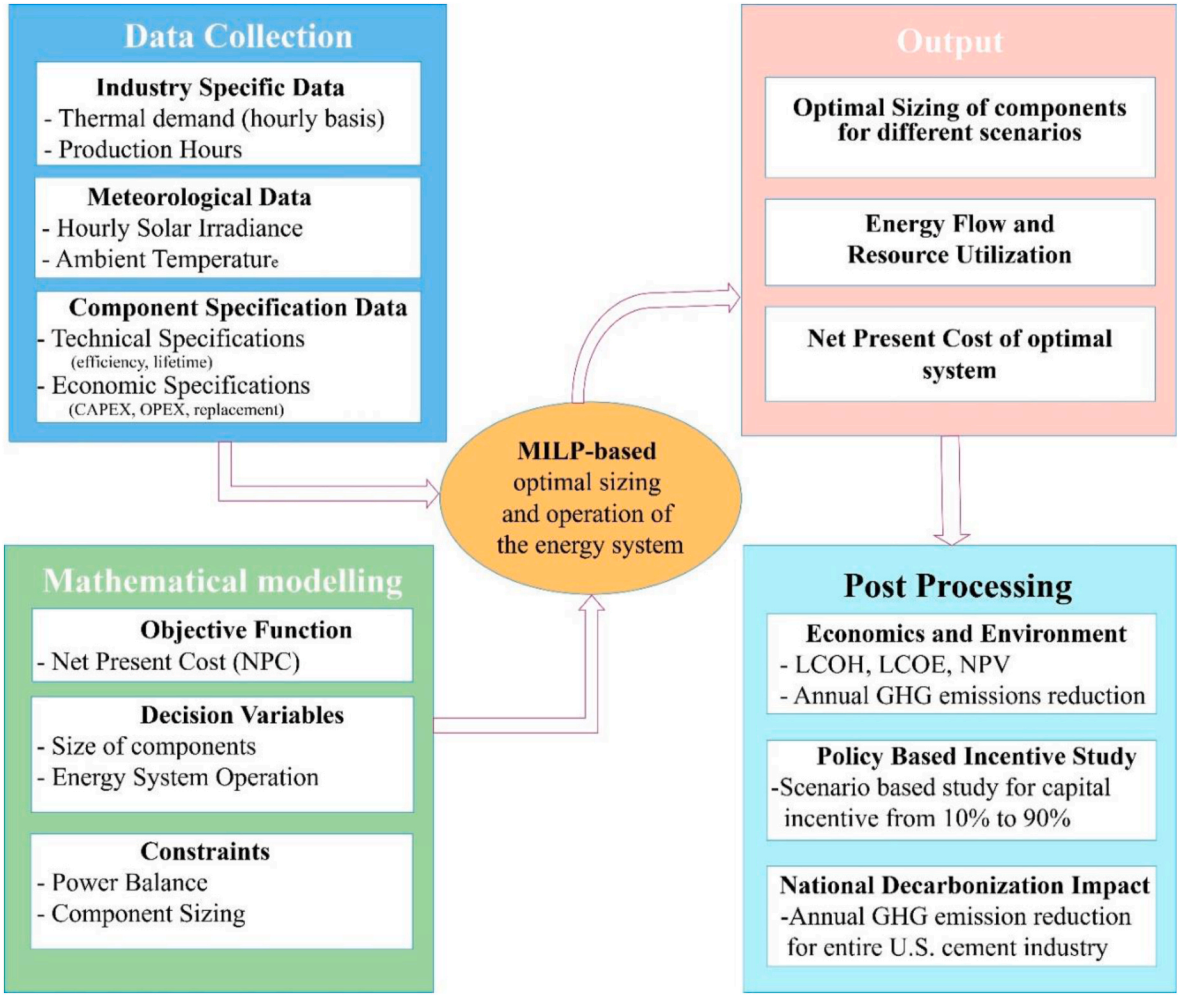


Fig. 1. Overall framework of the proposed research.

from industrial trials (Heidelberg Materials, 2024 [43]; MPA, 2022 [71]) showing stable combustion and clinker quality up to these substitution levels. A system-wide weighted cap of 35 % was therefore imposed in the model. The higher limit in the calciner is due to its lower operating temperature, secondary fuel flexibility, and separation from direct clinker formation reactions. The kiln's higher temperature and dependence on stable, controlled combustion for clinker formation make it more sensitive to hydrogen's high flame speed and low volumetric energy density. Excess hydrogen in the kiln can disrupt flame stability, increase NO_x emissions, and affect clinker quality, making lower blending ratios necessary [72]. Reported plant data show that the kiln with calciner, the energy consumption can vary from 40 to 60 %, depending on kiln size, fuel mix, and preheater configuration [73]. Based on this, a 50/50 energy split between the two units was assumed, with a maximum hourly hydrogen substitution cap of 35 %, calculated as weighted average. But maintaining the 35 % cap consistently year-round would require significant oversized PV and storage system to maintain that level during periods of low solar availability. To account for seasonal variability and infrastructure cost, an annual limit of 30 % on hydrogen substitution is imposed. For a representative cement plant considered in this study, this corresponds to 786,420 GJ/year of hydrogen energy, requiring 1,694,160 GJ/year of solar PV generation in 30 % substitution scenario. This annual cap therefore reflects a more practical, economically feasible target, while allowing operational flexibility under real-world conditions.

3.1. Data preparation

To ensure the study's relevance and scalability, we used a comprehensive dataset encompassing national clinker production figures (approximately 77 million metric tons annually) and regional solar resource data. Annual clinker production data from all U.S. plants were collected from the U.S. Geological Survey (USGS) and the Federal Reserve's G.17 Industrial Production and Capacity Utilization report. Analysis revealed the predominance of medium-sized cement plants. Therefore, we defined a representative model clinker production plant with a capacity of 2200 metric tons per day (TPD). This value represents the average clinker production capacity of U.S. plants, calculated by dividing the total U.S. clinker production by the number of operating plants. Scaling this model to 99 plants approximates the total clinker production of the U.S. cement industry. This provides a nationally relevant context for the findings. This model plant's hourly thermal energy consumption was determined by establishing a normalized 24-h profile based on existing literature [74] and scaled to reflect the 2200 TPD capacity to represent the typical daily variation. This profile was extrapolated on an annual basis as presented in Fig. 2a and b. The extrapolation incorporated factors like seasonal production variations (summer/winter), temperature-dependent adjustments (+0.3 % GJ/ton clinker per °C below 18 °C for winter heating losses and −0.15 % GJ/ton clinker per °C above 18 °C for summer efficiency gains), stochastic daily variability (±4–5 %), and planned maintenance shutdowns. The two pronounced anomalies observed on Fig. 2a at around 2000hrs and 6500hrs corresponds to scheduled 10-day maintenance periods modeled as reduced rate "hot hold" operation, where thermal input fell from 365 GJ/h to around 85 GJ/h, slowed by 75 %. This reflects the system being maintained at its minimum stable load to preserve refractory integrity and avoid the high restart penalty of a complete shutdown. The energy intensity in Fig. 2b remains within the typical range of 3.5–3.7 GJ/ton. Seasonal variability is evident: intensity decreases in summer due to reduced heat losses and drying needs and increases in winter from greater thermal demand.

The geographic location significantly impacts the feasibility of solar-powered hydrogen production due to variations in solar irradiance. While states like California and Missouri were considered, Texas was selected as the representative location for its optimal combination of high solar irradiance and substantial cement production capacity. This "sweet spot" ensures the study's relevance to a significant portion of the U.S. cement industry, balancing strong renewable energy potential with high industrial demand. California, while having excellent solar resources, has a lower cement production capacity than Texas. Missouri, on the other hand, has a lower solar irradiance than Texas. Hourly solar irradiance and ambient temperature data for these regions were obtained from the National Renewable Energy Laboratory's (NREL) System Advisor Model (SAM) software. The cement industries are assumed to have sufficient land area for PV installations. Other required parameters required for the calculation of PV power were taken from PV model titled SunPower SPR-E19-310-COM and are listed in Table 1. These data allow for accurate estimations of solar power generation potential and inform the optimal sizing of renewable hydrogen production systems. The temperature coefficient (α) below indicates how a solar panel's efficiency decreases as temperature rises, while the derating factor (f_{pv}) accounts for real-world losses (like dust, wiring, and shading) that reduce a panel's output below its rated capacity.

To evaluate the economic feasibility of integrating green hydrogen, a

Table 1
Parameter for solar PV system.

Parameter	Value	Reference
Nominal Operating Cell Temperature (NOCT)	46 ° C	[75]
Cell temperature at standard condition, $T_{cell,std}$	25 ° C	[75]
Temperature Coefficient, α	−0.00386 1/K	[75]
Incident irradiation at standard condition, G_{std}	1 kW/m^2	[75]
Derating Factor, f_{pv}	0.86	[76]

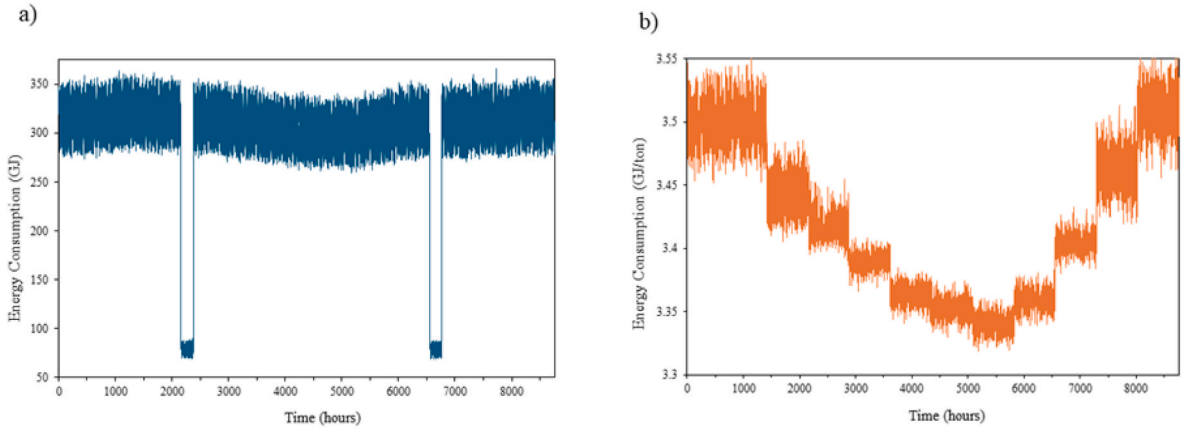


Fig. 2. (A) Hourly thermal energy consumption (GJ) profile in clinker kiln in entire year. **(b)** Hourly thermal energy consumption per ton of clinker (GJ/ton).

comprehensive cost analysis was conducted, covering both capital expenditures (CAPEX) and operational expenditures (OPEX). CAPEX accounts for the investment in photovoltaic (PV) systems, proton exchange membrane (PEM) electrolyzers (including balance-of-plant components), high pressurized hydrogen storage tank (up to 700 bars) [77], and the necessary infrastructure upgrades required for hydrogen integration within the cement plant. OPEX, derived from industry data and existing literature, includes ongoing maintenance, periodic replacement of key components such as PV panels, electrolyzer stacks, and hydrogen storage, as well as daily operational expenses associated with hydrogen production. PV system costs incorporate all essential auxiliary components, while hydrogen storage costs include piping and installation expenses. Electrolyzer costs cover both the stack and balance-of-plant components, including the water supply system, gas separator, and control mechanisms. In line with standard techno-economic assessment practices, maintenance costs were estimated as a percentage of CAPEX to ensure consistency and comparability across different hydrogen production scenarios. The parameters for electrolyzer performance and economic modeling were obtained from recent studies published between 2020 and 2024, as detailed in Tables 2 and 3.

3.2. Mathematical modeling for each system component

Fig. 3 illustrates the entire solar powered hydrogen production process implied to the clinker production, corresponding to the energy system operation and power balance phase under mathematical modelling section in Fig. 1. Raw materials undergo crushing, enter the pre-calciner and kiln, where coal provides heat. Hydrogen from solar-powered electrolysis is stored and used in the burner as a partial fuel replacement, reducing fossil fuel dependency and emissions. There are two major nodes N1 and N2, where major power balances take place. Node N1is responsible for ensuring that solar power must be equal or more than that required for electrolyzer to operate and node N2 ensures that power from hydrogen and coal must equal the total thermal energy need.

3.2.1. PV module

The power output generated by the solar photovoltaic (PV) system is determined using Eq. (1) [70],

$$P_{pv}(t) = f_{pv} \cdot P_{pv,rated} \cdot \left(\frac{G(t)}{G_{std.}}\right) \cdot \left(1 + \alpha \cdot \left(T_{cell}(t) - T_{cell,std}\right)\right) \quad (1)$$

where f_{pv} is the PV derating factor, $P_{pv,rated}$ is the rated PV capacity, $G(t)$ (kW/m^2) is the solar irradiance incident on the PV array at any time step of t, G_{std} is the incident solar irradiance under the standard test condition (STC), α (1/K) is the temperature coefficient, while $T_{cell,std}(t)$ (°C) corresponds to the PV cell temperature under STC, and 't' belongs to [1,T]. $T_{cell}(t)$ (°C) is the PV cell temperature at any given time calculated using Eq. (2) [76,90,91].

$$T_{cell}(t) = T_{amb}(t) + \frac{G(t)}{800}(NOCT - 20) \quad (2)$$

where $T_{amb}(t)$ is the ambient temperature at time t, and $NOCT$ refers to the nominal operating cell temperature. The $\left(1+\alpha\cdot\left(T_{cell}(t)-T_{cell,std}\right)\right.$ is also called temperature factor denoted by f_t and $\left(\frac{G(t)}{G_{std.}}\right)$ is the GHI factor $g_{(t)}$.

Table 2
Parameter for electrolyzer module.

Parameter	Value	Reference
Efficiency (BOP) η_{el}	0.81	[78]
Higher heating value of hydrogen, HHV_{H_2}	39.39 kWh/kg 141.8 MJ/kg	[79]
Minimum operating load, $y_{el,min}$	10 %	[77]
Maximum operating load, $y_{el,max}$	100 %	[77]

Table 3
Techno-economic assumptions.

Parameter	Value	Reference
Electrolyzer		
CAPEX	1188 $/kW	[77]
OPEX	7.5 % of CAPEX	[80]
Stack replacement cost	35 % of CAPEX	[77]
System installation cost	12 % of overall CAPEX	[80]
PV system		
CAPEX	981 $/KW	[78]
OPEX	1 % of CAPEX	[78,81]
Hydrogen storage		
CAPEX	480 $/kW	[77]
OPEX	2 % of CAPEX	[77]
Specific consumption	4 MJ/kg_{H2}	[77]
Efficiency of compressed hydrogen storage tank (η_{st})	0.95	[82]
Burner conversion cost	$200,000 per burner	[71]
Discount rate	10 %	[80]
System lifetime	20 years	
Stack life	10 years	
Cost of coal	$0.22 per kg/$8.6 per GJ/ $0.031/kWh	[83]
Electricity price	$0.16 per kWh	[84]
Oxygen price (Ambit, Frontier)	$0.08 per kg	[85]
GHG emission factor for coal, $EF_{GHG\ fuel}$	346 kg $CO_{2\ eq}$ per MWh of energy from coal 96 kg $CO_{2\ eq}$ per GJ	[86,87]
Grid electricity emission factor, $EF_{GHG_{grid}}$	425 kg $CO_{2\ eq}$ per MWh of energy	[88,89]

3.2.2. Electrolyzer

For this study, we propose a proton exchange membrane electrolyzer (PEMEL) for its compact size, operational feasibility and low start-up time. The rate of hydrogen produced per hour through this electrolyzer is given by Eq. 3

$$\dot{m}_{H_2} = \frac{P_{el} \cdot \eta_{el}}{HHV_{H_2}} \quad (3)$$

where, $\dot{m}_{H_2}$ is the rate of hydrogen produced in kg/hr, P_{el} is the power requested (in Watts) by the electrolyzer, η_{el} is the overall efficiency of electrolyzer along with auxiliary components such as water purification, cooling systems, compressors, valves etc., also called Balance of Plant (BoP) and HHV_{H_2} is called the higher heating value of the hydrogen which is given 141.8 MJ/kg. This is essential as the efficiency of the electrolyzer producing hydrogen is universally benchmarked against HHV. In order to maintain effective operation of the electrolyzer, the proposed system must switch from on and off based on the availability of sufficient power to operate from the solar PV. To incorporate switching, a binary variable $x(t)\ \epsilon\ [0,1]$, is introduced, where 0 means electrolyzer is not operating and 1 means electrolyzer is operating. Directly incorporating this binary control into the model through a product of $x(t)$ and continuous variable, $P_{el,rated}$, introduces a non-linearity, complicating the optimization process. So, to linearize we use an auxiliary variable $P_{el,rated,aux}$ to represent the non-linear term as is Eq. (4).

$$P_{el,rated,aux}(t) = P_{el,rated} \cdot x(t) \quad (4)$$

where $P_{el,rated}$ is the rated power of the electrolyzer and x(t) is a binary variable. In order to allow $P_{el,rated,aux}(t)$ accurately represent $P_{el,rated} \cdot x(t)$ without introducing nonlinearity, we impose constraints as shown by Eqs. (5)–(8).

$$P_{el,rated,aux}(t) \le P_{el,rated} - (1 - x(t)) \cdot P_{el,rated,min} \quad (5)$$

$$P_{el,rated,aux}(t) \ge P_{el,rated} - (1 - x(t)) \cdot P_{el,rated,max} \quad (6)$$

$$P_{el,rated,aux}(t) \le P_{el,rated,max} \cdot x(t) \quad (7)$$

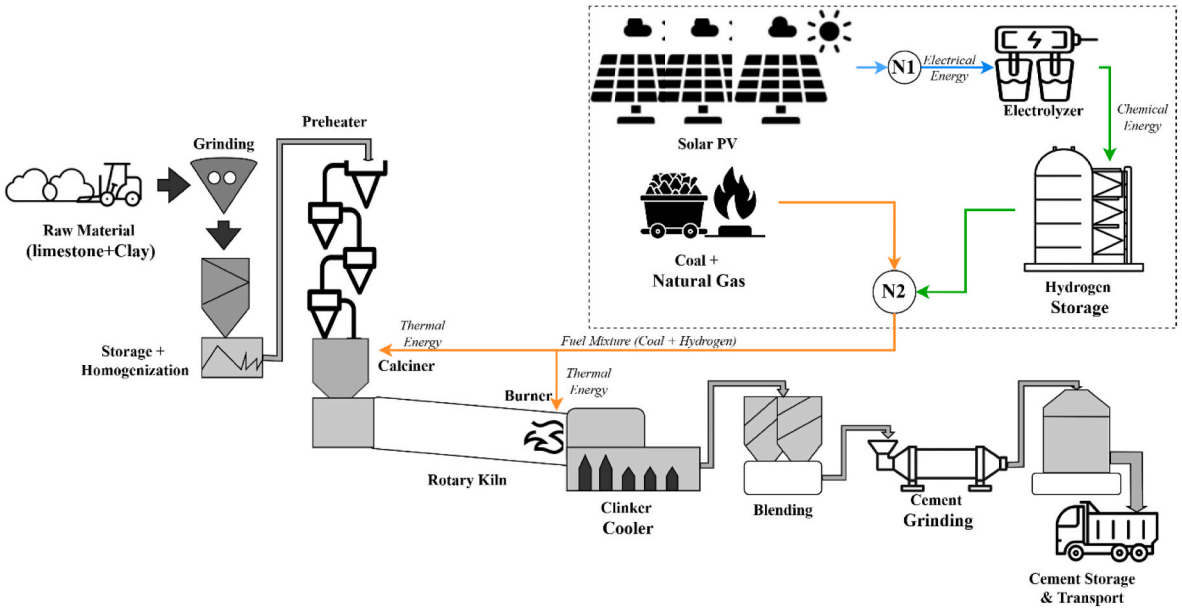


Fig. 3. Process overview for on-site hydrogen generation and utilization in cement plant.

$$P_{el,rated,aux}(t) \geq P_{el,rated,min} \cdot x(t) \tag{8}$$

These constraints collectively enforce the correct relationship between the binary control variable x(t) and the auxiliary variable $P_{el,rated,aux}(t)$, ensuring linearity in the model. When $x(t)$ is equal to 0, Eq. (5) and Eq. (7) reduce the upper bounds so that $P_{el,rated,aux}(t)$ is constrained to zero, meaning the electrolyzer is OFF. But when $x(t) = 1$, Eq. (6) and Eq. (8) activate and force the auxiliary variable, $P_{el,rated,aux}(t)$, become equal to $P_{el,rated}$, thus activating the electrolyzer at full rated capacity. To operate the electrolyzer at its minimum to its maximum operating range, we impose the constraint given in Eq. 9

$$y_{el,min} \cdot P_{el,rated,aux}(t) \leq P_{el} \leq y_{el,max} \cdot P_{el,rated,aux}(t) \tag{9}$$

where $y_{el,min}$ and $y_{el,max}$ are the lower and upper limit of the electrolyzer operating range. This constraint keeps the power used by the electrolyzer (P_{el}) within the operating range.

3.2.3. Hydrogen storage module

The hydrogen from the electrolyzer is first stored in the tank for storage and from there, supplied to the burner. Eq. (11) gives the hydrogen power produced by electrolyzer.

$$P_{H2,prod}(t) = P_{el}(t) \cdot \eta_{el} = \dot{m}_{H_2}(t) . HHV_{H_2} \tag{11}$$

where $P_{H2,prod}(t)$ is the hydrogen power produced in kW per time step as the electrolyzer operates at kW per time step. The entirety of this power is used to charge the hydrogen tank as given by Eq. (12),

$$P_{(ht,in)}(t) = P_{H2,prod}(t) \tag{12}$$

At each time step of 1 h, the hydrogen energy contained in tank ($HECT$) is given by Eq. (13).

$$HECT(t+1) = HECT(t) + P_{(ht,in)}(t) - \frac{P_{hf}(t)}{\eta_{st}} \tag{13}$$

where P_{hf} is the hydrogen power input (kW) into the thermal system and η_{st} is the efficiency of hydrogen storage tank. This efficiency incorporates the losses during storage, retrieval and other inefficiencies. Although $P_{el}(t)$ and $P_{hf}(t)$ are expressed in power units (kW), the equations are interpreted on a per-timestep basis, where the time resolution is 1 h. These power values effectively represent energy flows in kilowatt-hours (kWh) per timestep, making HECT consistent in units of energy (kWh). A boundary condition is implied for the first timestep of the simulation given as

$$HECT(0) = HECT_{rated} * LOH_{in} \tag{14}$$

where LOH_{in} is the level of hydrogen (LOH) of the storage tank at the beginning of the simulation and $HECT_{rated}$ is the rated capacity of the hydrogen tank. To limit the energy that can be stored in the storage tank, inequality constraint as defined earlier is given by Eq. 15

$$LOH_{min} HECT_{rated} \leq HECT(t) \leq LOH_{max} HECT_{rated} \tag{15}$$

Since, LOH_{min} is 0 and LOH_{max} is 1, the $HECT(t)$ can range from zero to its rated capacity $HECT_{rated}$.

3.2.4. System thermal load

The hydrogen stored in the tank is used to satisfy the thermal requirements of both the kiln and the calciner. The power output to the thermal system in each timestep is limited by a maximum percentage of the total hydrogen share required and total thermal load in the system, as given in Eq. (16).

$$P_{hf}(t) \leq w * P_{load}(t) \tag{16}$$

where w is the hourly percentage share in the fuel mix and $P_{load}(t)$ is the total thermal energy input into the system in that hour. In this study, the hydrogen share is limited to a maximum of 35 % of the total fuel input per timestep. Within this limit, the calciner's fuel consists of up to 45 % hydrogen, while the kiln uses up to 25 % hydrogen. For a representative case of 272 GJ total fuel demand per hour (136 GJ/h each for kiln and calciner), this corresponds to a maximum of 61 GJ/h hydrogen in the calciner and 34 GJ/h in the kiln, which is 95 GJ/h or 35 % of the system input. This cap is consistent with literature indicating that cement chemistry remains stable up to 35 % hydrogen substitution. The burners for both the calciner and the kiln are replaced, each incurring a capital expenditure (CAPEX) of $200,000 and an operational expenditure (OPEX) equal to 2 % of the CAPEX [71].

3.2.5. Power balance

In each time interval t of the simulation, two main power balances must be satisfied. The first power balance, which takes place in between solar PV and electrolyzer shown by N1 in Fig. 3, is given by Eq. 17

$$P_{pv}(t) \geq P_{el}(t) \tag{17}$$

where $P_{pv}(t)$ is the power generated by the solar PV. This inequality allows hours with PV output exceeding the electrolyzer load. To explicitly account for this surplus, A non-negative surplus curtailment term, $P_{curt}(t)$ is added, which has no value in the MILP objective. Thus, Eq. (17) can be written as Eq. 18

$$P_{pv}(t) = P_{el}(t) + P_{curt}(t) \tag{18}$$

where $P_{curt}(t)$ is $\left(P_{pv}(t) - P_{el}(t)\right) \geq 0$. This modelling approach was used as it helps the model to characterize H_2 supply costs and sizing independent of incentivizing PV over builds for grid-export benefits. After the optimization, the annual surplus energy $\left(\sum_{t=1}^{8760} P_{curt}(t)\right)$ is multiplied with a user specified fraction $\varnothing_{sell}$ (0.8 for our case) for grid sales in post processing.

The second power balance (N2) occurs in between the hydrogen storage tank and burner in the system where the power from the hydrogen and from the other fuel must always be equal to the total thermal energy required in the system in every time step "t" and is given as Eq. (19).

$$P_{load}(t) = P_{hf}(t) + P_f(t) \tag{19}$$

where $P_f(t)$ is the power generated by fuels other than hydrogen. Along with the power constraints, we implement a constraint that defines the annual hydrogen production/consumption target and is given as Eq. (20).

$$P_{yearly,H2} = x^* \sum_{t=1}^{8760} \mathrm{P}_{\mathrm{load}}(t) \tag{20}$$

where x is the variable share factor of hydrogen in total annual thermal load into the system. This share factor can be adjusted to create different scenarios for analysis, allowing us to examine how varying hydrogen production goals impact the system.

3.3. Analysis

A MILP optimization model was developed spanning one year, with the time horizon discretized into hourly intervals. The decision variables are divided into primary and auxiliary sets. The primary variables define the rated capacities of the system components, which include.

- $P_{pv,rated}$: The rated installed capacity of the PV array (kW)
- $ELOHT_{rated}$: The rated capacity of the hydrogen storage tank (kWh)
- $P_{el,rated}$: The rated power capacity of the electrolyzer (kW)

Auxiliary variables represent operational states at each time step t ∈ T (time horizon).

- $P_{pv}(t)$: Power output from the solar PV array (kW)
- $P_{el}(t)$: Power consumption of the electrolyzer (kW)
- $ELOHT(t)$: Energy stored in the hydrogen storage (kWh)
- $P_f(t)$: Power input into the thermal system (kWh)
- $\dot{m}_{H_2}(t)$: Mass flow rate of hydrogen produced by the electrolyzer (kg/s)

A binary variable to model the on-off state of the electrolyzer at each time step was employed, thereby incorporating operational constraints and potential startup/shutdown costs.

The objective function of this research is to minimize the Net Present Cost (NPC) of the overall renewable hydrogen production system over its operational lifecycle. It is defined as the sum of the capital expenditure of the plant (CAPEX) and the net operating expenditure (OPEX) and is expressed by Eq. (21).

$$\min_x NPC = CAPEX_{total} + OPEX_{total} \tag{21}$$

where $CAPEX_{total}$ is the sum of all the capital expenditure for all components involved in the system and $OPEX_{total}$ is the total annual operational and maintenance cost, discounted to their present value. Eq. (22) represents all capital cost including solar PV, electrolyzer installation cost, Hydrogen tank storage and burner conversion cost, while Eq. (23) present the net operating expenditure of the mentioned system components.

$$CAPEX_{total} = CAPEX_{PV} + CAPEX_{EL} + CAPEX_{HT} + CAPEX_{burners} \tag{22}$$

$$OPEX_{total} = \sum_{n=1}^{N} \frac{OPEX_{PV} + OPEX_{EL} + OPEX_{HT}}{(1+r)^n} \tag{23}$$

where n is a certain year over the lifetime of plant N, r is the discount rate.

The sizes of the PV array, electrolyzer and hydrogen storage system are treated as continuous decision variables, bounded within specific range, given by Eq. (24) and Eq. (25).

$$\mathrm{P}_{pv,\mathrm{rated,min}} \leq \mathrm{P}_{pv,\mathrm{rated}} \leq \mathrm{P}_{pv,\mathrm{rated,max}} \tag{24}$$

$$\mathrm{P}_{\mathrm{el,rated,min}} \leq \mathrm{P}_{\mathrm{el,rated}} \leq \mathrm{P}_{\mathrm{el,rated,max}} \tag{25}$$

where $\mathrm{P}_{pv,\mathrm{rated}}$ and $\mathrm{P}_{\mathrm{el,rated}}$ are the rated installed capacity of the PV array and the electrolyzer, respectively. The subscripts "min" and "max" denote the lower and upper bounds for each component's capacity, ensuring that the optimization model searches for solutions only within these specified limits.

The MILP model generates a comprehensive set of outputs that provide detailed insights into the optimal design and operation of the solar PV-based hydrogen production system. These outputs include the optimal rated capacities for the solar PV array and the electrolyzer unit, ensuring that hydrogen production meets demand at the lowest possible cost. The model also offers an in-depth understanding of the electrolyzer operational dynamics by specifying it's on/off status for each hour throughout the year. This information is crucial for analyzing the interplay between hydrogen production, solar energy availability, and hydrogen storage levels. The model delivers an hourly energy flow analysis, detailing the power generated by the solar PV array, the energy consumed by the electrolyzer, and the flow of hydrogen to the storage tank. From the hydrogen tank, the stored hydrogen is supplied to the cement kiln and clinker production processes. The excess electrical energy from solar PV, if any, is sold to the grid, contributing to additional revenue streams. These outputs form the foundation for further post-processing analysis, including the calculation of the levelized cost of hydrogen (LCOH), the levelized cost of energy (LCOE), and the estimation of CO_2 emission reductions achieved through this system. This comprehensive analysis also helps determine the economic viability and environmental benefits of integrating solar PV-based hydrogen production into industrial applications like cement manufacturing.

3.4. Economic metrics

Main economic metric derived from the optimization result is the LCOH. LCOH represents the average cost per unit of hydrogen produced over the system's lifetime, considering both capital and operational costs. The LCOH (in $/GJ) is given by Eq. (26).

$$LCOH = \frac{NPC_{H_2} - NPC_{revenue}}{\sum_{n=1}^{N} \left(\frac{M_{H_2}}{(1+r)^n}\right)} * 0.1418 \tag{26}$$

where M_{H_2} is the total hydrogen production in kg, $NPC_{revenue}$ is the sum of revenue that is collected from selling oxygen and 80 % of generated

electricity to the grid but at a fixed price.

3.5. Environmental metrics

The environmental impact is assessed by estimating the greenhouse gas (GHG) emissions, including carbon dioxide (CO_2), methane (CH_4), and nitrous oxide (N_2O), associated with the annual consumption of carbon-based fuels. Emissions are expressed in carbon dioxide equivalents (CO_2eq) using 100-year Global Warming Potential (GWP) values from the IPCC Fourth Assessment Report (AR4), with GWPs of 1 for CO_2, 25 for CH_4, and 298 for N_2O [92]. The yearly GHG savings (in CO_2eq) achieved through hydrogen utilization are calculated based on the annual energy demand met by hydrogen and the GHG emission factor of the substituted fuel.

The excess energy generated by the solar PV system, which is sold to the grid, contributes to further GHG reductions by displacing fossil-fuel-based electricity generation. Since grid electricity has its own GHG footprint, the substitution of conventional power with clean solar energy leads to indirect emission savings by preventing emissions that would have been produced by coal or natural gas power plants. The total GHG savings, represented by Eq. (27), include both direct reductions from fuel substitution and indirect reductions from renewable electricity export.

$$GHG_{savings} = E_{H2,year} \cdot EF_{GHG,fuel} + E_{excess,year} \cdot EF_{GHG_{grid}} \quad (27)$$

where, $E_{H2,year}$ is the annual energy demand fulfilled through hydrogen (kWh), $E_{excess,year}$ is the annual excess energy exported to the grid (kWh), $EF_{\mathrm{GHG}\ fuel}$ and $EF_{GHG_{grid}}$ are the GHG emission factor of the substituted fuel (kg CO_2eq/kWh) combustion and emission factor provided for grid electricity production respectively.

To relate these environmental benefits to techno-economic performance, the cost of CO_2 avoided is also calculated which is given in Eq. (28).

$$C_{CO_2,avoided} = \frac{NPC_{H_2} - NPC_{revenue} - NPC_{baseline}}{GHG_{svg,total}} \quad (28)$$

where, $NPC_{baseline}$ is the net present cost of the coal-only baseline, $GHG_{svg,total}$ is the cumulative GHG savings over a period of time which can be calculated by multiplying the annual GHG savings by the number of years.

4. Results

The performance of the proposed solar PV-powered hydrogen production system for cement manufacturing was evaluated through a comprehensive techno-economic analysis. The technical analysis consisted of mathematical modeling to optimize the entire system by determining the optimal sizing of PV, electrolyzer, and storage, while dynamically balancing hydrogen production and utilization to minimize net present cost (NPC). The results encompass an in-depth assessment of how system operates, optimal sizing for different hydrogen scenarios, financial viability, environmental impact, and policy-driven feasibility study.

Fig. 4 presents a time-series analysis of the system over a representative 164-h period, illustrating the dynamic interaction between system components within the cement industry. The PV generation, shown in Fig. 4a, follows a distinct diurnal cycle, peaking during daylight hours and ceasing at night. The electrolyzer's operation follows this pattern, utilizing available solar power to produce hydrogen. This relationship causes the electrolyzer to experience operational fluctuations, running

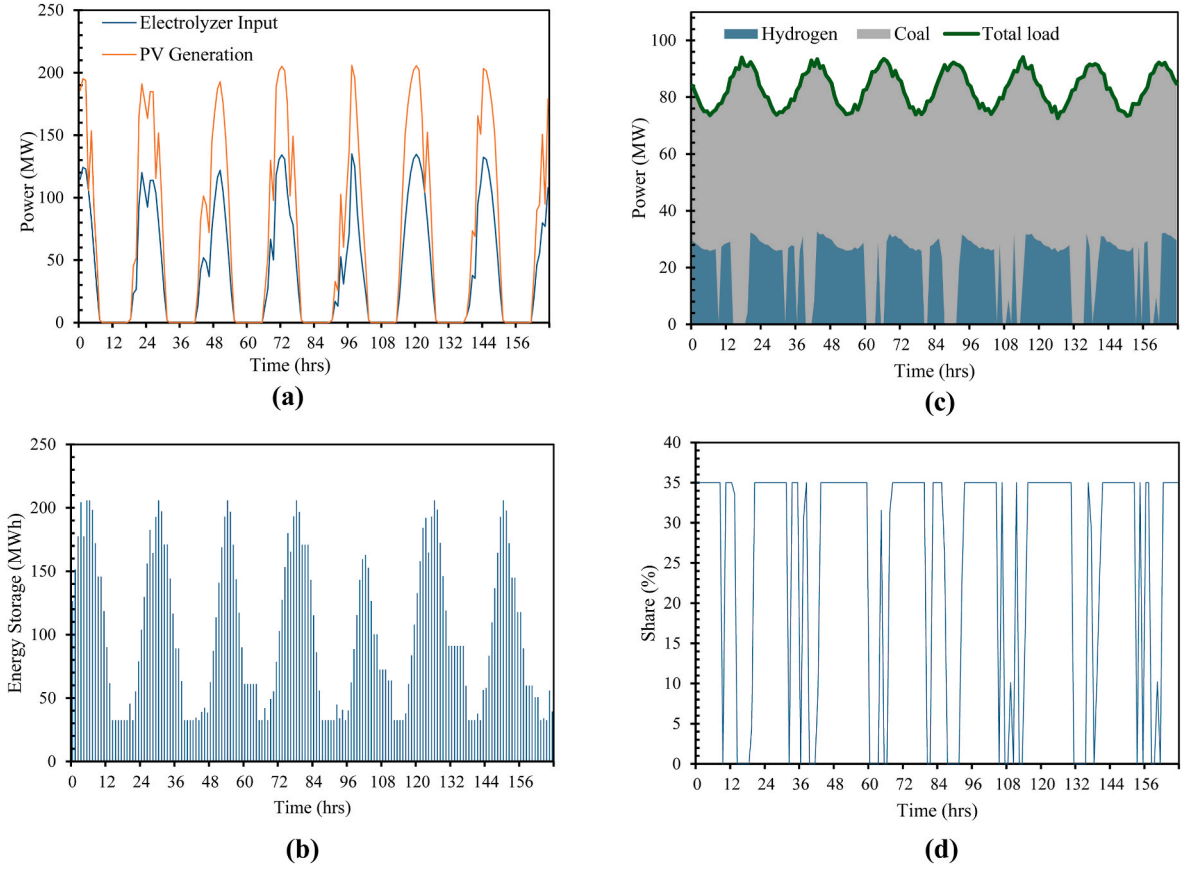


Fig. 4. Annual operational profile of a 20 % hydrogen shared production system. (a) Electrolyzer power input versus PV generation. (b) Hydrogen storage energy levels. (c) Power distribution across hydrogen, coal, and total load. (d) Annual hydrogen shares in total generation.

at partial load or shutting down entirely when solar generation falls below required thresholds. Since hydrogen production is inherently linked to solar availability, effective energy storage management becomes crucial for maintaining a consistent industrial supply. Fig. 4b shows the relationship between PV output and hydrogen storage, with the tank filling during periods of peak solar generation. The operational strategy of this system emphasizes immediate utilization of produced hydrogen, alongside concurrent storage. Because the cement plant's annual hydrogen demand is limited to 10–30 % and is largely met at the point of production, the need for substantial long-term storage is minimized. The storage tank primarily serves as a buffer to smooth out operational fluctuations, rather than functioning as a long-term energy reservoir. Nevertheless, scaling up the hydrogen share necessitates a corresponding increase in storage capacity to provide sufficient hydrogen during periods of low or no solar irradiance and ensure the achievement of the annual hydrogen usage target. Fig. 4c illustrates how hydrogen's contribution to the energy mix fluctuates based on electrolyzer activity and storage levels. When hydrogen reserves are depleted, coal automatically compensates to maintain a consistent energy supply. During non-solar days, when no hydrogen is produced, and the energy mix relies entirely on coal. This is particularly evident in winter months when solar generation is lower, causing the cement plant to rely exclusively on coal for thermal energy needs. Fig. 4d shows the variation in hydrogen share over time, confirming that it remains below the 35 % threshold per timestep, as designed in the optimization model. This controlled hydrogen-coal balance ensures uninterrupted plant operation, allowing the system to function efficiently throughout the year while integrating renewable energy sources wherever possible. As hydrogen integration in the system increases, it impacts system design, component sizing, and cost-effectiveness.

Table 4 presents the optimized capacities of the solar PV array, electrolyzer, and hydrogen storage system for different hydrogen share scenarios (10 %–30 %), along with the corresponding annual hydrogen production, associated Levelized Cost of Hydrogen (LCOH) and the cost of CO_2 avoided. A clear scaling trend is observed, as the hydrogen share increases, the required capacities of PV generation, electrolyzers, and storage grow substantially. At a 10 % hydrogen share, the plant produces 1848 metric tons of hydrogen annually, operating without storage and relying on real-time utilization with an 85 MW PV array and a 37 MW electrolyzer. As the hydrogen share rises to 30 %, the PV size expands to 337 MW, and electrolyzer capacity reaches 114 MW, requiring 493 MWh of hydrogen storage to balance supply with annual demand of 5545 metric tons of H_2. The necessity of storage at 15 % hydrogen shares and above suggests that real-time utilization alone is insufficient beyond this level. From a cost perspective, the LCOH increases from $58.67/GJ at 10 % to $95.27/GJ at 30 %. As the hydrogen share increases, system requirement changes disproportionately with larger PV panels, electrolyzers, and storage infrastructure. The resulting total investment cost rises nonlinearly with this capacity expansion, which drives the upward trend of LCOH. The cost increase is more pronounced beyond 15 % hydrogen share, likely due to reduced hydrogen production efficiency, higher storage needs, and increased operational complexity.

To connect techno-economic outcomes with environmental performance, the cost of CO_2 avoided was also quantified. Results show that this metric ranges from approximately $168/tCO$_2$ at 10 % substitution to $232/tCO$_2$ at 25 %, with a slight decline to $208/tCO$_2$at 30 % due to higher revenues from electricity exports. These values indicate that while higher hydrogen shares increase overall system costs, the abatement cost of CO_2 remains broadly within the midrange ($50-$200 tCO_2) reported for other industrial decarbonization strategies, highlighting both the potential and the policy support needed for solar-driven hydrogen in cement production.

Table 5 presents the instantaneous power balance of each component of the system at a specific timestep $t = 4000\ h$, selected as a representative mid-year daytime hour when solar availability is relatively high (GHI = 538 W/m^2) and temperature is moderate (35.7 °C). This hour reflects typical operating conditions when photovoltaic (PV) generation, electrolyzer operation, and storage dynamics are simultaneously active. The kiln–calciner system requires 272 GJ/h (75.7 MW) of thermal energy at this time, supplied by a mix of coal and hydrogen. A fixed upper bound of 35 % hydrogen share corresponds to 95 GJ/h of hydrogen demand, with the remaining 177 GJ/h provided by coal. The table compares energy flows across annual hydrogen-share scenarios under identical operating conditions to illustrate variability in system performance.

The energy for the system originates from the PV, whose performance is governed by the incoming solar irradiance and correction factors for ambient temperature and derating. For the 20 % scenario, a 195 MW PV array receives 538 W/m^2 of solar input, translating to 195 × 3.6 × 0.538 = 377 GJ/h of incident solar energy. After applying the derating and inverter efficiency factors (0.86 × 0.86), the useable PV output becomes 289 GJ/h. The electrolyzer then converts a portion of this AC power into hydrogen, with its electricity demand met entirely by the PV output. At this timestep, the electrolyzer consumes 71 × 3.6 = 255 GJ/h of electricity, producing 207 GJ/h of hydrogen ($\eta_{el} = 0.81$). Accounting for storage efficiency ($\eta_{st} = 0.0.95$), 196 GJ/h is received by the storage system, the difference representing compression losses. Of this, 95 GJ/h is supplied to the kiln, while the remaining 101 GJ/h is stored for later use. In the 10 % scenario, the optimized system does not generate sufficient hydrogen during this hour; the electrolyzer output directly feeds the kiln and calciner, supplying 92 GJ/h (out of 95 GJ/h required), with the shortfall met by coal. To account for technical and market constraints, only 80 % of surplus electricity is considered exportable to the grid, while the remaining fraction represents on-site use or handling losses.

At lower substitution levels, storage activity is minimal, and electrolyzer production nearly equals kiln–calciner hydrogen demand. As substitution caps increase, electrolyzer output and PV capacity grow rapidly, and the role of storage becomes more significant in balancing hourly mismatches. Table 5 therefore illustrates the detailed energy flows at the timestep level, showing how storage losses, PV oversizing, and grid sales interact to maintain the targeted hydrogen share without exceeding the kiln demand constraint. A complete power balance for each timestep under annual hydrogen-share scenarios of 10 %, 20 %, and 30 % is provided in the **Supplementary File**.

The Net Present Cost (NPC) analysis, as shown in Fig. 5, further reinforces these economic challenges. As hydrogen integration increases, the total system cost rises, driven mainly by investments in solar PV,

Table 4
Results for different values of hydrogen share (HS).

Hydrogen share (%)	PV Size (MW)	Electrolyzer size (MW)	H_2 storage size (MWh)	Annual H_2 production (metric tons)	LCOH ($/GJ)	Cost of CO_2 avoided ($/t$CO_2$)
10	85	37	0	1848	58.67	168
15	144	52	83	2772	67.98	171
20	195	71	216	3697	82.44	209
25	246	90	365	4621	91.33	232
30	337	114	493	5545	95.27	208

Capacities from optimization model (Eqs. (1)–(20)). H_2 production based on HHV = 141.8 MJ/kg. LCOH from Eq. (23); tCO_2e avoided cost from Eq. (27) using coal EF = 0.096tCO_2e/GJ and grid EF = 0.118 tCO_2e/GJ.

Table 5
Instantaneous energy and power balance at model timestep t = 4000 h, GHI is 538 w/m^2 and temperature of 35.7 °C.

Total Energy Demand	H_2 Scenario (%) (annual)	Coal Fuel Energy Demand	H_2 Energy Demand	H_2 Storage discharge	ΔE_{st}, Storage net change	H_2 Storage Charge	Electro-lyzer Output	Electro-lyzer Input	PV Output	PV input	Installed PV capacity (MW)	Physical excess	Sold to grid
272	10	180	92	92	–	92	97	120	127	166	85	7	5
272	15	177	95	95	50	145	153	188	213	278	144	25	20
272	20	177	95	95	101	196	207	255	289	377	195	34	27
272	25	177	95	95	154	249	262	324	357	476	246	33	26
272	30	177	95	95	218	314	330	408	500	653	337	92	73
*Per time step hydrogen fuel mix (**w**)*	–	–	**0.35** of system demand	-	-	-	-	-	-	-	-	-	-
Storage charge efficiency (η_{st})	–	–	-	-	-	**0.95**	-	-	-	-	-	-	-
Electrolyzer efficiency (η_{el})	–	–	-	-	-	-	**0.81**	-	-	-	-	-	-
Temperature factor (f_t)	–	–	-	-	-	-	-	-	**0.89**	-	-	-	-
Derating factor (f_{pv})	–	–	-	-	-	-	-	-	**0.86**	-	-	-	-
GHI factor ($g_{(t)}$)	–	–	-	-	-	-	-	-	-	**0.538**	-	-	-
MW to GJ conversion	–	–	-	-	-	-	-	-	-	**3.6**	-	-	-
Physical excess	–	–	-	-	-	-	-	-	-	-	-	**(PV_{out} – Ele_{in})**	-
Grid sell factor	–	–	-	-	-	-	-	-	-	-	-	-	**0.8 of excess**

All energy values are in GJ/h unless otherwise specified. PV output = Installed PV capacity × 3.6 × GHI × temperature factor × derating factor. Values represent the instantaneous system state for the illustrated hour (not annual averages). Coal and Hydrogen use higher heating values.

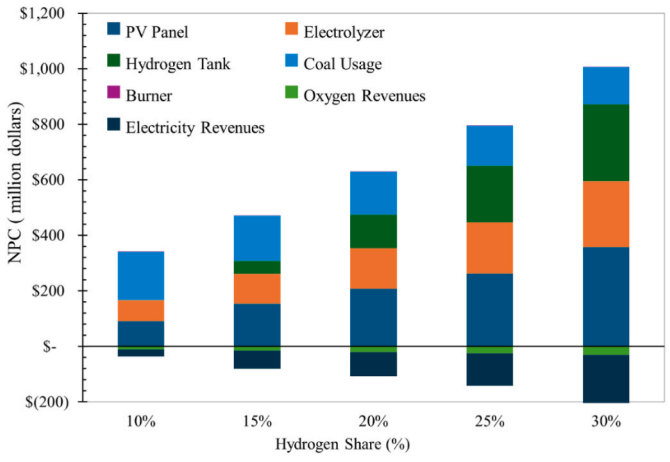
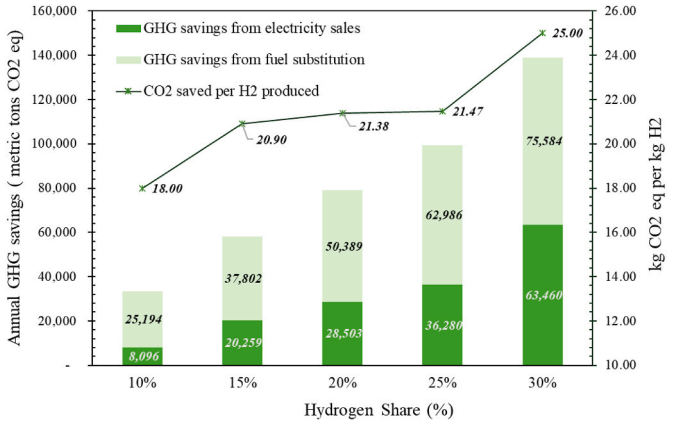


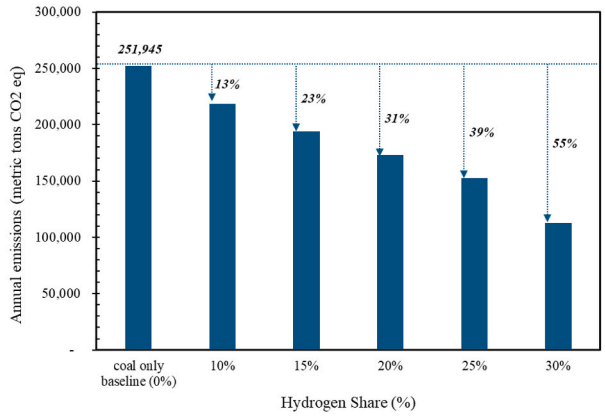
Fig. 5. NPC of the system at different hydrogen share percentage.

electrolyzers, and storage. While coal costs decrease with higher hydrogen use, declining from $173 million at 10 % hydrogen share to $134 million at 30 %, these savings do not fully offset the higher CAPEX requirements of the hydrogen system. Storage, in particular, becomes a major cost driver, adding $46 million at 15 % hydrogen share and rising to $277 million at 30 %. Despite the higher upfront costs, revenues from electricity and oxygen sales help recover some of the investment. The ability to sell 80 % of excess electricity to the grid provides an important revenue stream, though it does not fully counterbalance the rising LCOH at higher shares. This suggests that moderate hydrogen integration (10–20 %) remains the most financially sustainable option, as it minimizes storage costs while still reducing coal dependency. Beyond 25–30 %, further hydrogen adoption becomes increasingly expensive, requiring policy incentives or cost reductions in electrolyzer and storage technologies to remain viable. Hydrogen integration up to 30 % is technically feasible, scaling beyond this would require improvements in storage efficiency, lower cost electrolyzers, and industrial modifications. The ability of cement kilns and burners to handle higher hydrogen fractions is a crucial limitation, as modifications to combustion systems may be necessary. These factors emphasize the need for a balanced approach, where technological readiness, cost-effectiveness, and industrial feasibility align for a smooth transition toward cleaner cement production.

While the economic feasibility of hydrogen integration remains a crucial factor, its potential for reducing GHG emissions is equally important. The GHG savings from hydrogen integration in cement production increase significantly as the hydrogen share grows, driven by two key factors: coal substitution and excess renewable electricity sales to the grid. Both contributions are expressed in the same unit of avoided emissions (tCO_2e/year or metric tons CO_2e/year), using emission factors of 0.096 tCO_2e/GJ for coal (0.346 tCO_2e/MWh) and 0.118 tCO_2e/GJ for grid electricity (0.425 tCO_2e/MWh). As shown in Fig. 6a, at 10 % hydrogen share, total annual GHG savings amount to 33,290 metric tons, with 25,194 metric tons coming from direct coal displacement and 8096 metric tons from electricity sales. As hydrogen integration increases to 30 %, total GHG savings more than quadruple with 139,043 metric tons, with fuel substitution accounting for 75,584 metric tons and electricity sales contributing 63,460 metric tons, indicating a strong support from excess solar electricity displacing fossil-fueled grid power. This upward trend demonstrates that as more hydrogen replaces coal, total GHG emissions decline sharply, offsetting the plant's coal-only baseline of 251,945 metric tons per year by 13 % in the 10 % hydrogen scenario and a remarkable 55 % in the 30 % scenario as shown by Fig. 6b.



(a)



(b)

Fig. 6. (A) Avoided emissions from fuel substitution and grid-export credits, **(b)** annual emission comparison with baseline, expressed in tCO_2e/year.

The efficiency of hydrogen in cutting emissions improves at higher rates. The GHG savings per kg of hydrogen produced rises from 18 kg CO_2eq at 10 % to 25 kg CO_2eq at 30 %, suggesting that as the system scales, hydrogen is being used more effectively to offset emissions. Achieving these higher savings requires larger PV, electrolyzer, and storage investments, increasing system costs. While the environmental benefits are clear, financial feasibility remains a challenge, making policy incentives like carbon credits or subsidies essential. These results highlight that hydrogen adoption not only helps decarbonize cement production but also contributes to broader grid emissions reductions, reinforcing the need for a balanced approach between environmental impact and economic viability.

Fig. 7 presents NPC calculated for different hydrogen shares for different percentage of incentives (10 %–90 %). For this study, these incentives are applied as investment tax credits that are applied to the CAPEX of the entire hydrogen production system including PV array, electrolyzer cost and hydrogen storage. This study is carried out to analyze how crucial role policy support plays to make the green hydrogen production a cost-effective and viable solution. At 10 % hydrogen share, increasing incentives from 10 % to 90 % reduces NPC from $327 M to $224 M, a 32 % reduction in total system cost. At 30 % hydrogen share, NPC drops from $936 M at 10 % incentives to $366 M at 90 % incentives, marking a 60 % decrease. The reduction is more pronounced at higher hydrogen shares due to larger infrastructure requirements for electrolyzers and hydrogen storage, both of which drive capital expenditures. Without strong financial support, hydrogen integration beyond 20 % remains a costly option, requiring substantial subsidies or tax credits to remain viable. The results indicate that

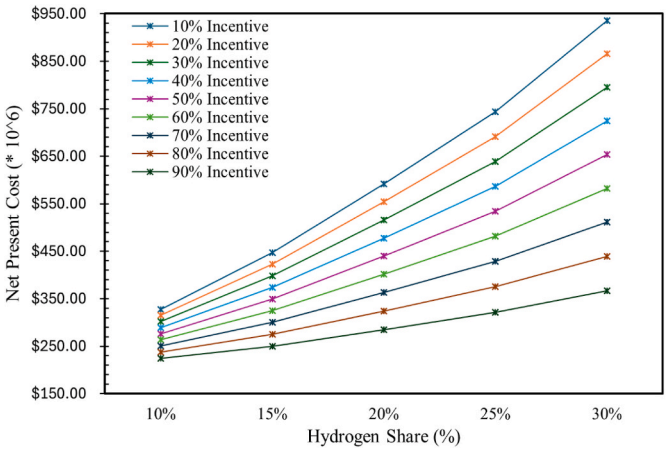


Fig. 7. Incentive based NPC at different hydrogen share percentage.

moderate hydrogen integration (10–15 %) is financially feasible with limited incentives, while higher penetration levels (25–30 %) require significant investment support to offset costs. Without these incentives, cement manufacturers would face high capital costs, limiting their ability to transition toward large-scale hydrogen adoption.

Fig. 8 presents a heatmap visualizing LCOH under various scenarios, varying both the percentage of hydrogen used in the fuel mix and incentive levels. Lighter shades indicate lower LCOH values, while darker shades represent higher costs. The LCOH values represent the total system cost over a 20-year period, accounting for revenue offsets from the sale of oxygen and electricity. Since these revenue streams contribute to lowering the net cost of hydrogen production, the LCOH values in the analysis reflect a different scenario, assuming revenue stability throughout the project's lifespan. Incentive levels of 70–90 % reflect optimistic scenarios, while 40–50 % reflect a realistic scenario. Incentive levels close to zero reflect worst case scenarios. Without incentives (0 % investment support), LCOH remains high, ranging from $58.67/GJ at 10 % hydrogen share to $95.27/GJ at 30 % hydrogen share. With 50 % incentives, LCOH declines to $27.78/GJ at 10 % share and $38.85/GJ at 30 % share. At 80 % investment incentive, the LCOH is $7.89/GJ for 10 % share and $0.21/GJ at 30 % share. The relationship between hydrogen shares and LCOH, however, demonstrates a nuanced behavior significantly influenced by the level of policy incentives. While a consistent decrease in LCOH is observed with rising investment incentives, the impact of hydrogen share is complex and non-linear. At higher incentive level, particularly from 40 % and higher, LCOH does not follow a strict upward path with increasing hydrogen share. This fluctuation contrasts with the steady increase observed at 20 % incentive, where LCOH rises consistently due to limited cost offsets and growing system requirements. The shift in behavior at higher incentives reflects the complex interplay between capital cost reductions, system sizing, and revenue recovery. As hydrogen share increases, the system requires larger PV arrays, electrolyzers, and storage, which grow non-linearly in cost and scale (Table 4). Between 15 % and 25 % hydrogen share, the additional storage capacity needed to maintain stable hydrogen supply (Fig. 5) results in a temporary increase in overall system cost. Reduced electrolyzer efficiency under partial load and increased cycling losses further raise LCOH in this range. Beyond this range, particularly at a 30 % hydrogen share, the larger infrastructure allows for improved utilization throughout the year, improving efficiency and allowing greater revenue offsets from electricity and oxygen sales. The resulting LCOH is therefore influenced not just by the amount of infrastructure added, but by how effectively that infrastructure is used within the optimized system. Understanding this dynamic is essential for evaluating the conditions under which green hydrogen becomes cost-competitive in the cement sector.

To assess economic viability, we compare the LCOH to the cost of

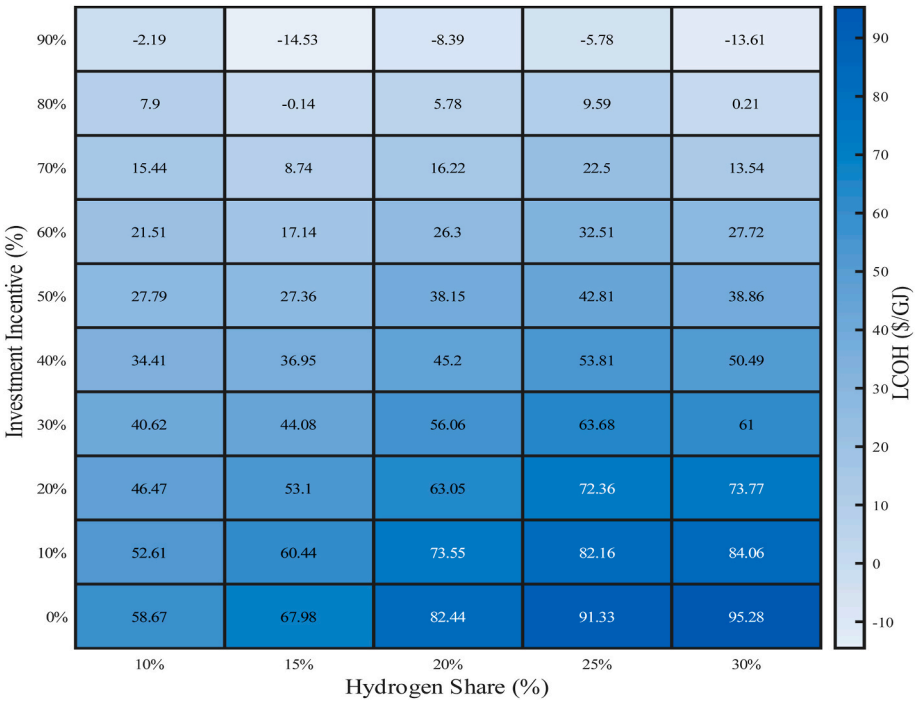


Fig. 8. Heatmap of LCOH at different hydrogen share percentage with different incentives.

carbon-based fuel. Conventional carbon fuel for cement industry is $8.6 per GJ. This appears higher as actual fuel cost in cement industry is elevated compared to spot commodity prices because of transport, onsite coal drying and grinding, handling losses, kiln efficiency, and ash disposal as per EPA [93]. Fig. 9 summarizes the LCOH at 10 % and 30 % hydrogen shares for different incentive levels and compares them to the benchmark coal price. Fig. 9 highlights the cost gap between hydrogen and coal. The LCOH without any revenue and capex investment credit, the gross LCOH is 9 times higher than coal baseline for 10 % and 15 times higher for 30 % scenarios. With revenue streams, the LCOH remains 7 to 11 times higher than coal, making hydrogen economically unviable. A 50 % incentive significantly lowers costs but still fails to achieve parity. At 80 % incentives, hydrogen at a 30 % share becomes 41 times cheaper than coal, marking a turning point where green hydrogen becomes a cost-effective alternative. The 90 % incentive scenario results in negative LCOH values for both hydrogen shares, indicating a net revenue generation due to the sale of oxygen and excess electricity. In parallel, the equivalent levelized cost of energy (LCOE), expressed on a $/GJ basis, follows the same trend since coal costs are fixed across scenarios. This highlights if these revenue credits fail to materialize as projected, the required financial incentive to achieve cost parity may exceed. The results clearly demonstrate a non-linear relationship between incentive levels, hydrogen shares, and LCOH. Higher hydrogen shares coupled with high incentives are crucial for achieving cost parity and, ultimately, cost superiority compared to coal. This analysis strongly suggests that policies promoting both investment in hydrogen production and its increased utilization in energy-intensive industries like cement manufacturing are essential for its successful integration into the energy mix.

Fig. 10 illustrates the relationship between investment incentives and annual GHG savings. While LCOH and NPC consistently decline as incentives increase, GHG savings remain largely unchanged. Slight variations were observed, where total GHG savings occasionally decrease with mid-range incentives. For instance, in the case of a 20 % hydrogen share, GHG savings dropped from 79,100 metric tons to a 10 % incentive to 78,900 metric tons at a 20 % incentive. Since this change is less than 2 %, it is rounded off and considered as no significant variation. These minor fluctuations result from system optimization adjustments and computational nuances, which remain negligible and do not alter the overall trend. At higher incentive levels (above 40 %), a slight increase in GHG savings is observed across all hydrogen shares. At the 70 % incentive level, GHG savings increased by approximately 100 metric tons (10 % hydrogen share), 900 metric tons (20 % hydrogen share), and 3800 metric tons (30 % hydrogen share) compared to the previous incentive level. This suggests that when financial incentives are sufficiently high, the optimization model may prioritize larger system sizes, leading to slightly greater emission reductions. GHG savings remain nearly constant as the incentive percentage increases, indicating that financial incentives primarily improve the economic feasibility of hydrogen adoption rather than directly affecting emissions. While the impact on a single facility may seem marginal, once the system becomes economically viable, large-scale implementation across the U.S. cement sector could result in significant emission reductions, supporting the industry's goal of achieving net-zero emissions by 2050.

This effect is quantified in Table 6, which provides an extrapolated national-scale assessment of GHG reductions achievable through fuel substitution with hydrogen in cement manufacturing. The data presented encompasses both direct emissions savings from displacing coal in the kiln and calciner, as well as indirect savings from exporting surplus renewable electricity to the grid.

Table 6 shows that increasing hydrogen integration leads to a proportional reduction in national cement sector emissions, with up to 29 % direct savings across US and up to 22 % total US cement sectoral emissions savings at 30 % hydrogen share. This proportional trend arises because hydrogen directly replaces the combustion-related CO_2 component while simultaneously lowering emissions through renewable electricity displacement. The results demonstrate that even partial hydrogen blending, when coupled with renewable power, can deliver meaningful sector-level abatement without compromising production continuity. As technology matures, increasing the hydrogen share beyond 30 % will unlock progressively greater emissions savings, accelerating the path toward deep industrial decarbonization. From an economic standpoint, this mitigation potential must be contextualized by the current cost disparity between green hydrogen and fossil fuels. While the environmental benefits are clear, achieving cost-effective implementation at scale hinges on addressing economic barriers. As

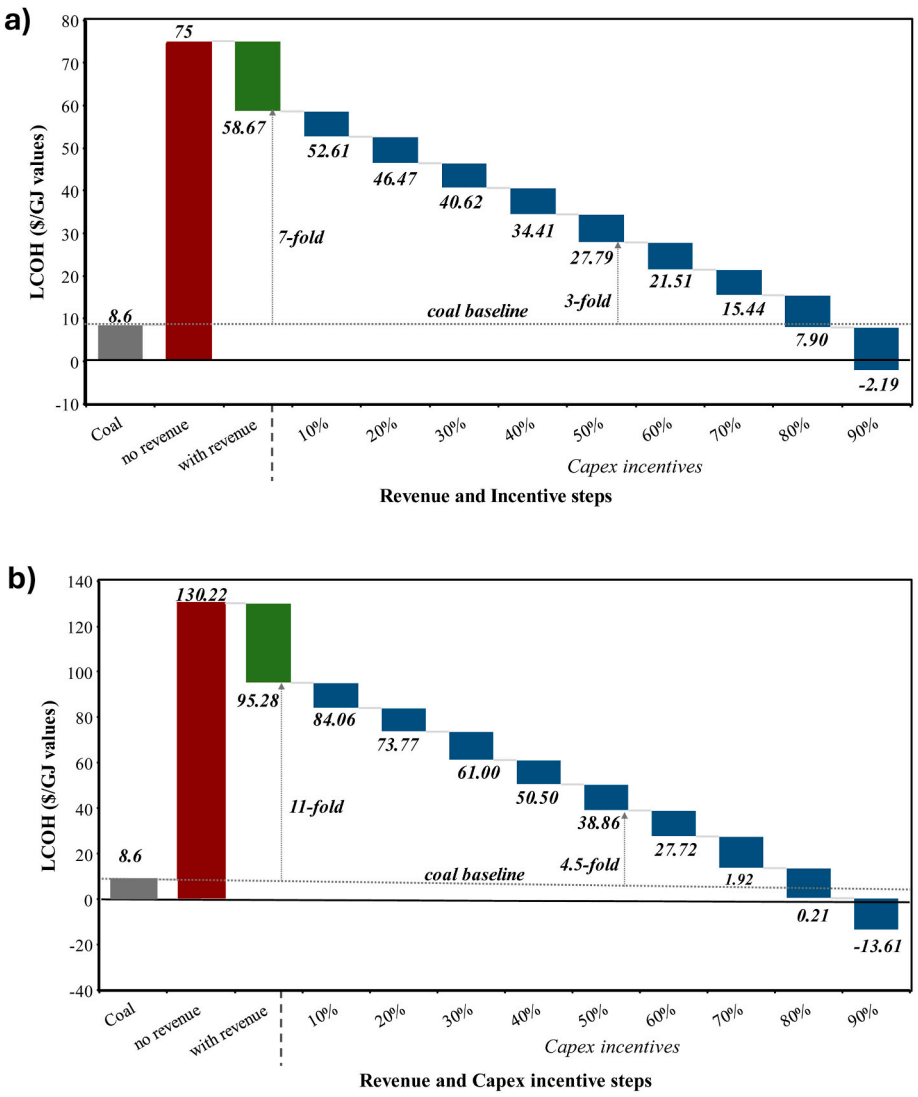


Fig. 9. LCOH comparison with coal. **a)** 10 % scenario **b)** 30 % scenario.

our analysis indicates, a substantial capital investment credit of 80 % or more is necessary to make hydrogen adoption financially competitive.

Compared to coal, substituting natural gas offers meaningful emissions reduction, thanks to its lower fuel emission intensity(fuel emission intensity of 53 kg CO_2/GJ compared to coal's 96 kg CO_2/GJ; EIA 2024 [86]). As a carbon-based fuel, natural gas cannot eliminate combustion-phase CO_2 entirely. Even at 100 % substitution, natural gas achieves only about 40 % emissions savings relative to coal. In contrast, hydrogen offers a fundamentally different pathway: when used as a substitute, it can virtually eliminate direct CO_2 emissions at the point of use. Thus, natural gas can may serve as a transitional solution for near-term emission mitigation. Hydrogen blending provides a true long-term net zero carbon pathway as it avoids any carbon leakage at the point of use. When viewed as part of a longer decarbonization strategy along with electrification and carbon capture, utilization, and storage (CCUS), hydrogen integration can serve as a cornerstone for achieving net zero emissions in cement sector. This transition can model how targeted policy incentives and technological advancements can accelerate progress toward net-zero goals in other hard-to-abate industries.

5. Conclusion

This study investigated the techno-economic feasibility of integrating on-site solar-powered green hydrogen production into U.S. clinker manufacturing, a critical pathway for decarbonizing this energy-intensive sector using a novel mixed-integer linear programming (MILP) model. Our technical analysis reveals the feasibility of hydrogen integration up to a 30 % annual share, but scaling hydrogen substitution necessitates substantial increases in PV array, electrolyzer, and particularly hydrogen storage capacities.

Economically, our findings underscore a significant cost hurdle. Levelized Cost of Hydrogen (LCOH) increases non-linearly with higher hydrogen shares, driven by escalating capital expenditures even with revenue streams from oxygen and electricity sales are considered. Green hydrogen remains significantly more expensive than conventional coal-based fuel. The cost of CO_2 avoided ranges from $168 to $232/t$CO_2$ placing solar driven hydrogen within the mid-range of industrial abatement costs, suggesting that moderate hydrogen substitution can already be justified but higher substitution requiring significant policy support.

Policy plays a critical role in bridging this economic gap. Our investment tax credit analysis shows that incentives of 80 % or higher are essential to achieving cost parity with coal. At 90 % incentives, the system can even generate net revenue, making large-scale adoption financially viable. While financial incentives primarily enhance economic feasibility, the environmental benefits are profound. Hydrogen substitution up to 30 % could reduce total GHG emissions from the U.S. cement sector by 22 %, a figure that would increase substantially with

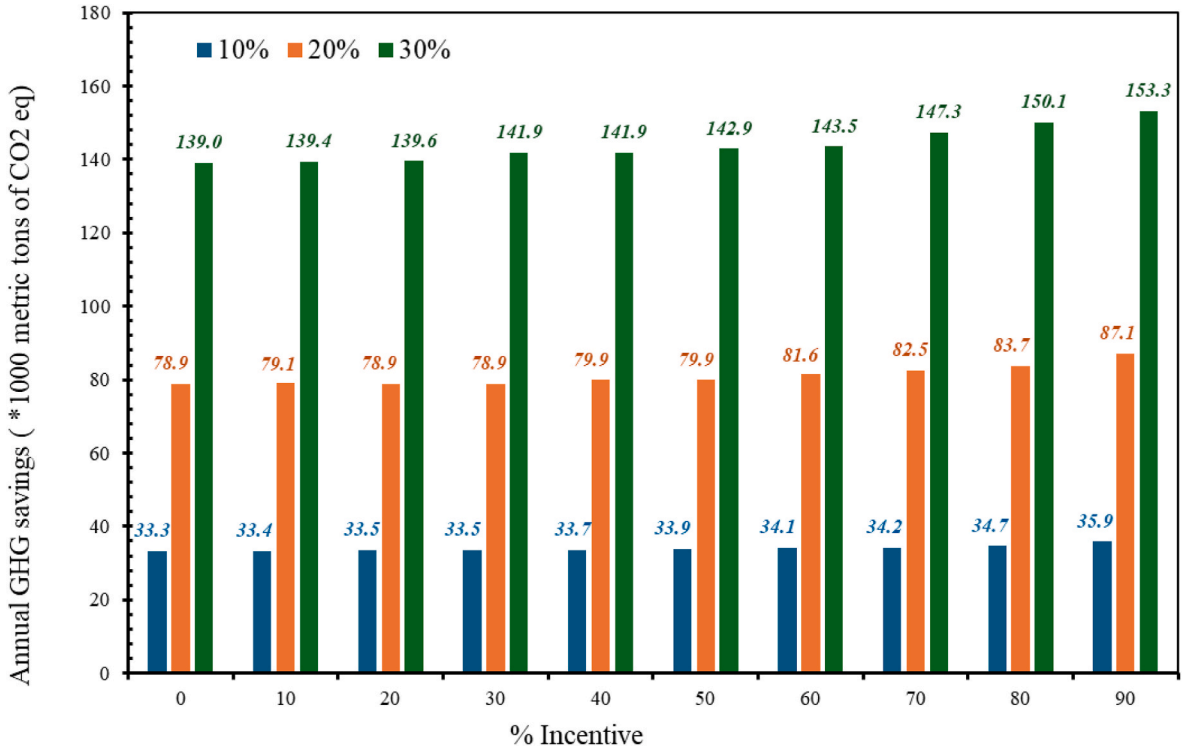


Fig. 10. Annual GHG savings at different hydrogen share percentage with different incentives.

Table 6
Decarbonization potential for entire US cement industry.

H_2 Share	Direct (fuel) ($ktCO_{2eq}$/yr. plant)	Indirect (Grid) (kt CO_{2eq}/yr. plant)	Total (kt CO_{2eq}/yr. plant)	U.S. total (Mt CO_{2eq}/yr)	% cut vs US cement sector	% cut vs Fuel comb. only
10 %	25	8	33	3.3	5 %	10 %
20 %	50	29	79	7.8	12 %	19 %
30 %	76	64	139	13.8	22 %	29 %

greater levels of substitution in the future.

The implications of this research extend beyond cement, demonstrating a potentially scalable techno-economic framework applicable to other hard-to-abate industrial sectors. This study provides a valuable starting point for evaluating the costs, benefits, and optimal design of integrated green hydrogen systems for industrial decarbonization. The necessity of policy intervention is evident, reinforcing the need for strategic government support to accelerate industrial decarbonization. A phased transition strategy, starting with moderate hydrogen integration and scaling up as technology advances and costs decline, emerges as the most pragmatic pathway for deep industrial decarbonization.

CRediT authorship contribution statement

Sobit Sapkota: Writing – review & editing, Writing – original draft, Visualization, Validation, Software, Methodology, Formal analysis, Data curation, Conceptualization. **Anup Paudel:** Writing – review & editing, Writing – original draft, Validation, Software, Methodology, Formal analysis, Conceptualization. **Wonjae Choi:** Writing – review & editing, Writing – original draft, Validation, Methodology. **Inyoung Ko:** Writing – review & editing, Validation. **Jun-Ki Choi:** Writing – review & editing, Writing – original draft, Validation, Supervision, Project administration, Methodology, Funding acquisition.

Declaration of competing interest

The authors declare that they have no known competing financial interests or personal relationships that could have appeared to influence the work reported in this paper.

Acknowledgement

The author would like to express gratitude to the US Department of Energy for supporting this work through their funding of the Industrial Assessment Center program (DE-EE0009721).

Appendix A. Supplementary data

Supplementary data to this article can be found online at https://doi.org/10.1016/j.ijhydene.2025.152508.

References

[1] Adesina A. Recent advances in the concrete industry to reduce its carbon dioxide emissions. Environ Chall 2020;1:100004.
[2] Scrivener KL, John VM, Gartner EM. Eco-efficient cements: potential economically viable solutions for a low-CO2 cement-based materials industry. Cement Concr Res 2018;114:2–26.
[3] Jaganmohan M. Portland and masonry cement production in the U.S. 2010-2023. Available from: https://www.statista.com/statistics/219329/us-production-of-portland-and-masonery-cement/; 2024.
[4] Rahman A, Rasul M, Khan M, Sharma S. Cement kiln process modeling to achieve energy efficiency by utilizing agricultural biomass as alternative fuels. In: Thermofluid modeling for energy efficiency applications. Elsevier; 2016. p. 197–225.
[5] Internationl Energy Agency. Low-carbon transition in the cement industry. IEA; 2018.
[6] Commission ET. Reaching net-zero carbon emissions from harder-to-abate sectors by mid-century. 2018.
[7] Andrew RM. Global CO 2 emissions from cement production. Earth Syst Sci Data 2018;10(1):195–217.
[8] Eash-Gates PK, Stefan Metz, Lucy Hittinger, Joe Hopkins, Asa S, Weiss Ida. Recasting the future: policy approaches to drive cement decarbonization. 2025. Boston, MA.

[9] Statista. Carbon dioxide emissions from global cement manufacturing. In: Million tons); 2025. Available from: https://www.statista.com/statistics/1091672/carbon-dioxide-emissions-global-cement-manufacturing/.
[10] Gao T, Shen L, Shen M, Liu L, Chen F. *Analysis of material flow and consumption in cement production process*. Journal of Cleaner Production 2016;112:553–65.
[11] Schakel W, Hung CR, Tokheim L-A, Strømman AH, Worrell E, Ramírez A. Impact of fuel selection on the environmental performance of post-combustion calcium looping applied to a cement plant. Appl Energy 2018;210:75–87.
[12] Czigler T, Reiter S, Schulze P, Somers K. Laying the foundation for zero-carbon cement, vol. 9. McKinsey & Company; 2020.
[13] Liu J, Zhang S, Wagner F. Exploring the driving forces of energy consumption and environmental pollution in China's cement industry at the provincial level. J Clean Prod 2018;184:274–85.
[14] Ige OE, Olanrewaju OA, Duffy KJ, Collins OC. Environmental impact analysis of Portland cement (CEM1) using the midpoint method. Energies 2022;15(7):2708.
[15] Wolde MG, Khatiwada D, Bekele G, Palm B. A life cycle assessment of clinker and cement production in Ethiopia. Cleaner Environmental Systems 2024;13:100180.
[16] Amran M, Makul N, Fediuk R, Lee YH, Vatin NI, Lee YY, Mohammed K. Global carbon recoverability experiences from the cement industry. Case Stud Constr Mater 2022;17:e01439.
[17] Bataille C, Åhman M, Neuhoff K, Nilsson LJ, Fischedick M, Lechtenböhmer S, Solano-Rodriquez B, Denis-Ryan A, Stiebert S, Waisman H. A review of technology and policy deep decarbonization pathway options for making energy-intensive industry production consistent with the Paris Agreement. J Clean Prod 2018;187:960–73.
[18] Hanifa M, Agarwal R, Sharma U, Thapliyal P, Singh L. A review on CO2 capture and sequestration in the construction industry: emerging approaches and commercialised technologies. J CO2 Util 2023;67:102292.
[19] Pisciotta M, Pilorgé H, Davids J, Psarras P. Opportunities for cement decarbonization. Cleaner Engineering and Technology 2023;15:100667.
[20] Cement G. Global cement and concrete Association. 2021.
[21] Sherif Z, Sarfraz S, Jolly M, Salonitis K. A critical review of the decarbonisation potential in the UK cement industry. Materials 2025;18(2):292.
[22] Imbabi MS, Carrigan C, McKenna S. Trends and developments in green cement and concrete technology. Int J Sustain Built Environ 2012;1(2):194–216.
[23] Fennell PS, Davis SJ, Mohammed A. Decarbonizing cement production. Joule 2021;5(6):1305–11.
[24] Kääntee U, Zevenhoven R, Backman R, Hupa M. Cement manufacturing using alternative fuels and the advantages of process modelling. Fuel Process Technol 2004;85(4):293–301.
[25] U.S. Department of Energy. Manufacturing Energy and Carbon Footprint: sector: cement (NAICS 327310). 2021.
[26] McNelly M, Choi J-K. Pathway to decarbonization through industrial energy efficiency: micro and macro perspectives from compressed air usage. International Journal of Precision Engineering and Manufacturing-Green Technology 2024;11(5):1575–91.
[27] Eardley S, Choi J-K, Hong T, An J. Decarbonization potential of regional combined heat and power development. Renew Sustain Energy Rev 2024;189:114038.
[28] Belaïd F. How does concrete and cement industry transformation contribute to mitigating climate change challenges? Resources, Conservation & Recycling Advances 2022;15:200084.
[29] Nnabuife SG, Hamzat AK, Whidborne J, Kuang B, Jenkins KW. Integration of renewable energy sources in tandem with electrolysis: a technology review for green hydrogen production. Int J Hydrogen Energy 2025;107:218–40.
[30] Paudel AP, Bishwash Mainali, Prasad Durga, Karki Sameep, Pochareddy Yashwanth, Shakya Shree Raj, Karki Seemant. Hydrogen production from surplus hydropower: Techno-economic assessment with alkaline electrolysis in Nepal's perspective. Int J Hydrogen Energy 2024;74.
[31] Newborough M, Cooley G. Developments in the global hydrogen market: the spectrum of hydrogen colours. Fuel Cell Bull 2020;2020(11):16–22.
[32] Gailani A, Cooper S, Allen S, Pimm A, Taylor P, Gross R. Assessing the potential of decarbonization options for industrial sectors. Joule 2024;8(3):576–603.
[33] Sarkar A, Banerjee R. Net energy analysis of hydrogen storage options. Int J Hydrogen Energy 2005;30(8):867–77.
[34] Winter C-J. Hydrogen energy—Abundant, efficient, clean: a debate over the energy-system-of-change. Int J Hydrogen Energy 2009;34(14):S1–52.
[35] Yue M, Lambert H, Pahon E, Roche R, Jemei S, Hissel D. Hydrogen energy systems: a critical review of technologies, applications, trends and challenges. Renew Sustain Energy Rev 2021;146:111180.
[36] Griffiths S, Sovacool BK, Kim J, Bazilian M, Uratani JM. Industrial decarbonization via hydrogen: a critical and systematic review of developments, socio-technical systems and policy options. Energy Res Social Sci 2021;80:102208.
[37] Yin Q, Du W-J, Cheng L. Optimization design of heat recovery systems on rotary kilns using genetic algorithms. Appl Energy 2017;202:153–68.
[38] Jibran JA, Mahat C. Application of green hydrogen for decarbonization of cement manufacturing process: a technical review. In: Journal of physics: conference series. IOP Publishing; 2023.
[39] Hercog J, Lewtak R, Glot B, Jóźwiak P, Nehring G, Tavares VD, Nunes AM, Gaspar D. Pilot testing and numerical simulations of the multifuel burner for the cement kiln. Fuel 2023;342:127801.
[40] Holcim. Climate Report 2021. 2021.
[41] Clark G, Davis M, Kumar A. Assessment of fuel switching as a decarbonization strategy in the cement sector. Energy Convers Manag 2024;312:118585.
[42] Becerra-Lopez HR, De Silva-Munoz L, Flores-Hernandez JR, Lira-Arguello R, Romero-Castanon T. *Forecasting regional green hydrogen demand in Mexico by 2035*. International Journal of Hydrogen Energy 2025;141:1039–49.
[43] Materials H. Annual and Sustainability Report 2023. 2024.
[44] Adu-Amankwah S, Douglas B, Arkless L, Cardinal N, Zajac M. Mixed hydrogen and biofuels cement clinker: characterisation, microstructure, and performance. Cement Concr Compos 2025;155:105814.
[45] Habib MA, Abdulrahman GA, Alquaity AB, Qasem NA. Hydrogen combustion, production, and applications: a review. Alex Eng J 2024;100:182–207.
[46] Schmidt N, Müller M, Preuster P, Zigan L, Wasserscheid P, Will S. Development and characterization of a low-NOx partially premixed hydrogen burner using numerical simulation and flame diagnostics. Int J Hydrogen Energy 2023;48(41):15709–21.
[47] Dai H, Zhang B, Li Z, Wu J. Combustion characteristics of a porous media burner with partial hydrogen injection. Int J Hydrogen Energy 2022;47(2):1092–102.
[48] Astbury G, Hawksworth SJ. Spontaneous ignition of hydrogen leaks: a review of postulated mechanisms. Int J Hydrogen Energy 2007;32(13):2178–85.
[49] Juangsa FB, Cezeliano AS, Darmanto PS, Aziz M. Thermodynamic analysis of hydrogen utilization as alternative fuel in cement production. South African Journal of Chemical Engineering 2022;42:23–31.
[50] Nhuchhen DR, Sit SP, Layzell DB. Decarbonization of cement production in a hydrogen economy. Appl Energy 2022;317:119180.
[51] Bacatelo M, Capucha F, Ferrão P, Margarido F, Bordado J. Carbon-neutral cement: the role of green hydrogen. Int J Hydrogen Energy 2024;63:382–95.
[52] Murphy Z, Kapp S, Choi J-K. Analytical study on daylight harvesting potential for manufacturing facilities: Techno-economic-environmental perspective. Energy Build 2024;320:114565.
[53] Ozturk M, Dincer I. Utilization of waste heat from cement plant to generate hydrogen and blend it with natural gas. Int J Hydrogen Energy 2022;47(48):20695–704.
[54] Rezaei M, Naghdi-Khozani N, Jafari N. Wind energy utilization for hydrogen production in an underdeveloped country: an economic investigation. Renew Energy 2020;147:1044–57.
[55] Rahil A, Gammon R, Brown N. Techno-economic assessment of dispatchable hydrogen production by multiple electrolysers in Libya. J Energy Storage 2018;16:46–60.
[56] Gallardo FI, Ferrario AM, Lamagna M, Bocci E, Garcia DA, Baeza-Jeria TE. A Techno-Economic Analysis of solar hydrogen production by electrolysis in the north of Chile and the case of exportation from Atacama Desert to Japan. Int J Hydrogen Energy 2021;46(26):13709–28.
[57] U.S. Department of Energy, *U.S.* In: Energy Do, editor. National clean hydrogen strategy and roadmap. Washington, D.C.: U.S. Department of Energy; 2023. p. 96.
[58] U.S. Department of the Treasury. Treasury sets out proposed rules for transformative clean hydrogen incentives. Available from: https://bidenwhitehouse.archives.gov/cleanenergy/tax-guidance-explainers/2023/12/22/treasury-sets-out-proposed-rules-for-transformative-clean-hydrogen-incentives/; 2023.
[59] Huneke F, Henkel J, Benavides González JA, Erdmann G. Optimisation of hybrid off-grid energy systems by linear programming. Energy, Sustainability and Society 2012;2:1–19.
[60] Denzinger C, Berkemeier G, Winter O, Worsham M, Labrador C, Willard K, Altaher A, Schuleter J, Ciric A, Choi J-K. Toward sustainable refrigeration systems: life cycle assessment of a bench-scale solar-thermal adsorption refrigerator. Int J Refrig 2021;121:105–13.
[61] Choi J-K, Paudel A, Karki B, Bradley K, Quinn N, Ciric A. Comprehensive reviews on technological and life cycle environmental aspects of solar–thermal adsorption refrigerator. Resources, Environment and Sustainability 2025;19:100195.
[62] Fthenakis V, Zhang Z, Choi JK. Cost optimization of decommissioning and recycling CdTe PV power plants. In: 2017 IEEE 44th photovoltaic specialist conference (PVSC); 2017.
[63] Nedaei M, Abtin A, Changkyoo Y, Jun-Ki C, Assareh E. The potential of wind for energy production and water pumping in Iran, Saravan County. Distr Generat Alternative Energy J 2016;31(1):7–26.
[64] Alsehli M, Alzahrani M, Choi J-K. A novel design for solar integrated multi-effect distillation driven by sensible heat and alternate storage tanks. Desalination 2019;468:114061.
[65] Ghareeb A, Nooruldeen O, Arslan CA, Kapp S, Choi J-K. Synergistic optimization of predictive models for water quality analysis in treatment plants using machine learning and evolutionary algorithms. Evolutionary Intelligence 2025;18(2):34.
[66] Choi J-K, Paudel A, Sapkota S, Alsehli M, Alshamrani A, Park J, Hong Y, Romeiko X. Comparative assessment of conventional and emerging desalination technologies: a holistic review for sustainable water solutions. Desalination 2025:119140.
[67] McLaughlin E, Choi J-K. Utilizing machine learning models to estimate energy savings from an industrial energy system. Resources, Environment and Sustainability 2023;12:100103.
[68] Naji A, Al Tarhuni B, Choi J-K, Alshatshati S, Ajena S. Toward cost-effective residential energy reduction and community impacts: a data-based machine learning approach. Energy and AI 2021;4:100068.
[69] Mohammed A, Ghaithan AM, Al-Hanbali A, Attia AM. A multi-objective optimization model based on mixed integer linear programming for sizing a hybrid PV-hydrogen storage system. Int J Hydrogen Energy 2023;48(26):9748–61.
[70] Paudel A, Choi J-K. Techno-economic pathway for green hydrogen adoption in thermal applications across US small and medium manufacturing sectors. Int J Hydrogen Energy 2025;98:295–307.
[71] Li, Ning, and Cise Unluer. "Towards a net zero built environment: decarbonisation of the UK cement industry." *npj Materials Sustainability* 3.1 (2025): 10.
[72] Boher C, Frizon F, Lorente S, Bart F. Influence of the pore network on hydrogen diffusion through blended cement pastes. Cement Concr Compos 2013;37:30–6.

[73] Waltisberg J, Weber R. Disposal of waste-based fuels and raw materials in cement plants in Germany and Switzerland–What can be learned for global co-incineration practice and policy? Emerging Contam 2020;6:93–102.
[74] Ali S, Malik TN, Raza A. Hybrid risk-averse energy management optimizer for large-scale industrial building microgrids. International Transactions on Electrical Energy Systems 2020;30(8):e12442.
[75] System advisor model. Golden, CO: National Renewable Energy Laboratory; 2024. p. 855–63.
[76] Marocco P, Ferrero D, Martelli E, Santarelli M, Lanzini A. An MILP approach for the optimal design of renewable battery-hydrogen energy systems for off-grid insular communities. Energy Convers Manag 2021;245:114564. 114564.
[77] Marocco P, Gandiglio M, Audisio D, Santarelli M. Assessment of the role of hydrogen to produce high-temperature heat in the steel industry. J Clean Prod 2023;388:135969. 135969.
[78] Park J, Kang S, Kim S, Cho HS, Heo S, Lee JH. Techno-economic analysis of solar powered green hydrogen system based on multi-objective optimization of economics and productivity. Energy Convers Manag 2024;299:117823. 117823.
[79] Vives AMV, Wang R, Roy S, Smallbone A. Techno-economic analysis of large-scale green hydrogen production and storage. Applied energy 2023;346:121333.
[80] Kim M, Lee D, Qi M, Kim J. Techno-economic analysis of anion exchange membrane electrolysis process for green hydrogen production under uncertainty. Energy Convers Manag 2024;302:118134. 118134.
[81] Bhandari R, Shah RR. Hydrogen as energy carrier: Techno-economic assessment of decentralized hydrogen production in Germany. Renew Energy 2021;177:915–31.
[82] Ni M. An overview of hydrogen storage technologies. Energy Explor Exploit 2006; 24(3):197–209.
[83] Analytiq B. Bituminous coal price index. Available from: https://businessanalytiq.com/procurementanalytics/index/bituminous-coal-price-index/; 2025.
[84] GridHacker. Solar buyback plans in Texas. Available from: https://www.gridhacker.com/resources/solar-buyback-plans-texas; 2024 2025.
[85] Analytiq B. Oxygen price index. Available from: https://businessanalytiq.com/procurementanalytics/index/oxygen-price-index/; 2025.
[86] U.S. Energy Information Administration. Carbon dioxide emissions coefficients by fuel. Available from: https://www.eia.gov/environment/emissions/co2_vol_mass.php; 2024.
[87] Farfan J, Fasihi M, Breyer C. Trends in the global cement industry and opportunities for long-term sustainable CCU potential for Power-to-X. J Clean Prod 2019;217:821–35.
[88] Carbon Footprint Ltd. Grid Electricity Emissions Factors v0.1 – january 2022: Country-Specific electricity grid greenhouse gas emission factors. 2021. 2022.
[89] Carbon Footprint Ltd. Grid electricity emissions factors v1.0. 2019. 2019.
[90] Li B, Roche R, Miraoui A. Microgrid sizing with combined evolutionary algorithm and MILP unit commitment. Appl Energy 2017;188:547–62.
[91] Singh A, Baredar P, Gupta B. Techno-economic feasibility analysis of hydrogen fuel cell and solar photovoltaic hybrid renewable energy system for academic research building. Energy Convers Manag 2017;145:398–414.
[92] IPCC. *Climate change 2014: mitigation of climate change. Contribution of Working group III to the fifth assessment report of the intergovernmental panel on climate change*. Fifth assessment report. Cambridge, United Kingdom and New York, NY, USA: Cambridge University Press; 2014.
[93] Associates JD, Nunenkamp DC. Coal preparation environmental engineering manual. Industrial Environmental Research Laboratory, Office of Research and; 1976.